

# BALM: A Model-Agnostic Framework for Balanced Multimodal Learning under Imbalanced Missing Rates

Phuong-Anh Nguyen, Tien Anh Pham, Duc-Trong Le, Cam-Van Thi Nguyen\*  
 VNU University of Engineering and Technology  
 Hanoi, Vietnam

{22028332, 23021696, trongld, vanntc}@vnu.edu.vn

## Abstract

Learning from multiple modalities often suffers from imbalance, where information-rich modalities dominate optimization while weaker or partially missing modalities contribute less. This imbalance becomes severe in realistic settings with imbalanced missing rates (IMR), where each modality is absent with different probabilities, distorting representation learning and gradient dynamics. We revisit this issue from a training-process perspective and propose **BALM**, a model-agnostic plug-in framework to achieve balanced multimodal learning under IMR. The framework comprises two complementary modules: the Feature Calibration Module (FCM), which recalibrates unimodal features using global context to establish a shared representation basis across heterogeneous missing patterns; the Gradient Rebalancing Module (GRM), which balances learning dynamics across modalities by modulating gradient magnitudes and directions from both distributional and spatial perspectives. BALM can be seamlessly integrated into diverse backbones, including multimodal emotion recognition (MER) models, without altering their architectures. Experimental results across multiple MER benchmarks confirm that BALM consistently enhances robustness and improves performance under diverse missing and imbalance settings. Code available at: [https://github.com/np4s/BALM\\_CVPR2026.git](https://github.com/np4s/BALM_CVPR2026.git)

## 1. Introduction

Multimodal learning has achieved substantial progress by jointly exploiting complementary information from audio, visual, and textual modalities [2, 20, 31, 47]. However, real-world multimodal systems rarely operate under perfect conditions, as sensor failures, recording noise, or acquisition costs often cause partial or complete modality loss [30, 46, 54]. This phenomenon leads to *incomplete*

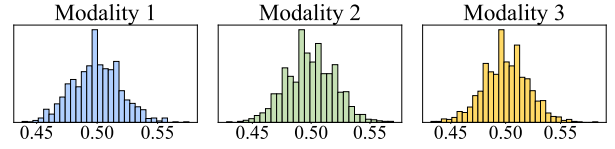


Figure 1. Modality-specific missing rates' distribution of a tri-modal dataset under Share Missing Rate (SMR=0.5).

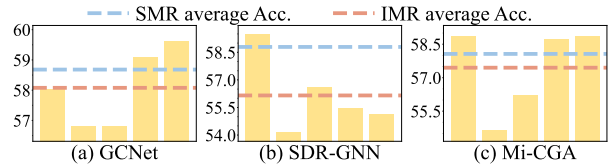


Figure 2. Model accuracy under SMR=0.5 and five equivalent IMR settings with  $(r_A, r_L, r_V) \in \{0.3, 0.5, 0.7\}$  on IEMOCAP.

*multimodal learning*, where missing data affect both representation quality and cross-modal interaction [54]. Effectively handling incomplete or missing modalities remains a central challenge for building reliable multimodal systems [21]. Beyond incompleteness, multimodal learning inherently faces *modality imbalance* [38, 45, 49], where modalities contribute unequally due to differences in signal reliability, feature granularity, and data scale. When modalities are missing, this imbalance worsens as the dominant modality overfits while the less frequent or corrupted ones receive limited supervision, leading to a biased equilibrium that weakens robustness and generalization.

Recent advances in missing-modality learning have explored two main paradigms to enhance robustness under incomplete data: *alignment-based methods*, which align representations between complete and incomplete inputs using contrastive, correlation, or augmentation techniques [19, 22, 28, 30], and *generation-based methods*, which reconstruct missing modalities through autoencoders, variational inference, graph reasoning, or diffusion models [26, 40, 50, 56]. These approaches generally overlook the imbalance

\*Corresponding author

that arises when missingness occurs during training. Notably, some models [7, 19] compute reconstruction losses using the full data, whereas some approaches [50, 56] do not employ reconstruction but rely on pretrained encoders trained on full modalities, leaving challenges of incomplete training data unaddressed.

Most prior studies further simplify the problem by adopting the *Shared Missing Rate (SMR)* assumption [7, 19, 56], where all modalities are randomly dropped with the same probability. As illustrated in Fig. 1, when  $SMR=0.5$ , each modality exhibits comparable missing proportions, resulting in a statistically balanced yet idealized setting. In contrast, realistic multimodal systems often encounter uneven data degradation across modalities due to heterogeneous acquisition or noise. We refer to this scenario as the *Imbalanced Missing Rate (IMR)* condition [33, 34, 55], which introduces persistent exposure disparity and optimization bias across modalities. As shown in Fig. 2, traditional missing-modality models exhibit unstable behavior under *IMR* settings, particularly when the missing rates across modalities differ significantly. This imbalance causes performance fluctuations, as models struggle to adapt when one modality becomes substantially less reliable than the others.

**Our approach.** We study multimodal learning under the *Imbalanced Missing Rate (IMR)* setting, where modality absence occurs from the beginning of training and follows distinct missing rates. Imbalanced Missing Rate introduces two coupled challenges: (1) *representation imbalance*, where heterogeneous missing patterns distort unimodal feature distributions and hinder consistent cross-modal fusion [36]; and (2) *learning imbalance*, where gradients are dominated by frequently observed modalities, leading to biased convergence [8]. To address these issues, we propose **BALM (Balanced Agnostic Learning under Imbalanced Missing Rates)**, a lightweight and model-agnostic plug-in framework that mitigates both representation- and optimization-level imbalance under *IMR*. Our propose BALM integrates seamlessly with existing multimodal backbones, particularly those used in MER. It comprises two complementary modules: a Feature Calibration Module (FCM) that aligns representations across varying missing patterns, and a Gradient Rebalancing Module (GRM) that harmonizes optimization dynamics by adaptively modulating gradient magnitudes and directions. Our main contributions are summarized as follows:

- We propose **BALM**, a plug-in framework that enables robust multimodal learning under the *Imbalanced Missing Rate* condition without redesigning existing architectures.
- We design two complementary modules: a *Feature Calibration Module (FCM)* for representation-level alignment and a *Gradient Rebalancing Module (GRM)* for optimization-level balancing.
- We conduct extensive experiments on multiple MER

benchmarks, showing that BALM consistently enhances robustness across standard backbones, imbalance-oriented models, and missing-modality methods.

## 2. Related Work

### 2.1. Incomplete Multimodal Learning

Recent studies on incomplete multimodal learning can be broadly categorized into two paradigms [54]. **Alignment-based methods** aim to bridge the gap between complete and incomplete inputs by aligning their latent representations. Contrastive objectives [18, 22] encourage modality-invariant embeddings, while correlation-based techniques such as canonical correlation analysis and its extensions [1, 10, 37] learn cross-modal coherence. Other efforts incorporate masking or noise-based augmentation [30, 51] to simulate missingness and improve robustness. Although effective at aligning feature spaces, these methods depend on balanced modality exposure and struggle under heterogeneous missing conditions. **Generation-based methods** explicitly reconstruct missing modalities to recover full-modality representations. Autoencoder-based frameworks [26, 35] learn deterministic mappings between observed and missing modalities, while variational inference models [39, 56] impose probabilistic constraints to improve generative consistency. Graph-based completion networks [19, 28] capture structural dependencies among modalities and instances, whereas diffusion-based approaches [4, 5, 41] leverage denoising priors to iteratively refine reconstructed signals. Despite their generative flexibility, these methods still assume identical missing probabilities across modalities and rarely consider imbalance during optimization.

### 2.2. Imbalanced Multimodal Learning

Imbalance in multimodal learning occurs when some modalities dominate training because they provide stronger or more reliable information [38, 45, 54]. This causes biased gradients and uneven representation learning, where dominant modalities are updated more effectively while weaker ones lag behind. Prior studies address this issue through data re-sampling [43], adaptive feature calibration [24, 54], objective regularization [24, 42, 48], and gradient modulation [14, 17, 27, 29, 44]. These approaches enhance cooperation among modalities when all are fully available. Under incomplete conditions, imbalance worsens as low-availability modalities provide fewer samples and gradients, slowing convergence and degrading representations. The interplay between modality imbalance and missing data further complicates optimization and weakens cross-modal alignment. Our work addresses these issues by jointly calibrating features and rebalancing gradients for stable learning under heterogeneous missing conditions.

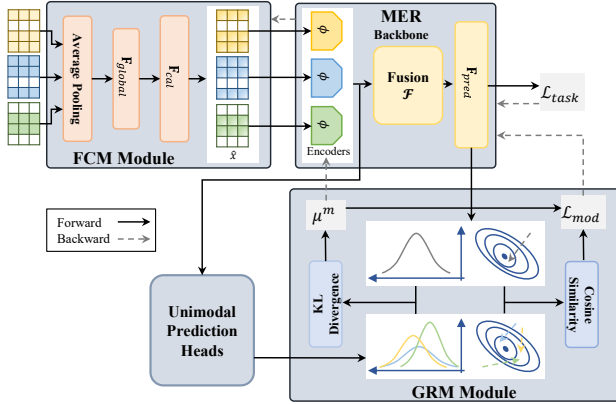


Figure 3. Overview of BALM, consisting of a Feature Calibration Module (FCM) and a Gradient Rebalancing Module (GRM) for balanced multimodal learning under imbalanced missing rates.

### 3. Methodology

Given a multimodal dataset  $\mathbb{D} = \{(x_i, y_i)\}_{i=1}^N$  with  $M$  modalities and label space  $\mathcal{Y}$ , the multimodal feature of sample  $i$  is denoted as  $x_i = \{x_i^m\}_{m=1}^M$ , where  $x_i^m \in \mathbb{R}^{d_m}$  represents the feature of modality  $m$ . To simulate missing-modality scenarios, we introduce a stochastic masking operator  $\mathcal{M}(\cdot; \mathbf{r})$  parameterized by a missing-ratio vector  $\mathbf{r} = [r_1, \dots, r_M]$ , where  $r_m \in [0, 1)$  denotes the probability that modality  $m$  is absent. The missing mask vector of a multimodal sample is obtained via  $e_i \sim \mathcal{M}(x_i; \mathbf{r})$ , where each observation indicator  $e_i^m \in \{0, 1\}$  indicates the availability of modality  $m$  for sample  $i$ . The indicator is generated with regards to the missing probability  $r_m$  while ensuring at least one modality is available for each sample. The incomplete dataset is defined as  $\tilde{\mathbb{D}} = \{(\tilde{x}_i, y_i)\}_{i=1}^N$ , where  $\tilde{x}_i$  is the incomplete multimodal sample with unimodal feature  $\tilde{x}_i^m = x_i^m$  if  $e_i^m = 1$ , and  $\tilde{x}_i^m = \vec{0}$  if otherwise.

#### 3.1. Shared- and Imbalanced Missing Rate

**Shared Missing Rate (SMR).** In the shared setting, all modalities follow the same Bernoulli missingness pattern, where for each sample  $i$  and modality  $m$ . The observation indicator  $e_i^m \in \{0, 1\}$  is drawn via  $P(e_i^m = 1) = 1 - r_{\text{shared}}$  and  $P(e_i^m = 0) = r_{\text{shared}}$ , with  $r_{\text{shared}} \in [0, 1)$  denoting the shared missing rate. The joint masking distribution is:

$$p_{\text{SMR}}(e) = \frac{\prod_{m=1}^M (1 - r_{\text{shared}})^{e^m} r_{\text{shared}}^{1-e^m}}{1 - r_{\text{shared}}^M}, \quad (1)$$

where  $e = \{e^m\}_{m=1}^M$  represents the binary masking pattern. Here, the denominator normalizes by excluding the all-missing case. For each modality  $m$ , the empirical missing ratio  $\hat{r}_m = \frac{1}{N} \sum_{i=1}^N (1 - e_i^m)$  follows a Binomial distribution

with expectation and variance:

$$\mathbb{E}[\hat{r}_m] = r_{\text{shared}}, \quad \text{Var}[\hat{r}_m] = \frac{r_{\text{shared}}(1 - r_{\text{shared}})}{N}. \quad (2)$$

As  $N$  increases,  $\hat{r}_m$  converges to  $\mathcal{N}(r_{\text{shared}}, \frac{r_{\text{shared}}(1 - r_{\text{shared}})}{N})$ , implying all modalities are statistically equivalent (see Fig. 1), and any difference among  $\hat{r}_m$  arises from stochastic fluctuation rather than systematic imbalance.

**Imbalanced Missing Rate (IMR).** In realistic multimodal environments, different modalities exhibit heterogeneous missing probabilities ( $r_m \neq r_{m'}$ ) due to sensor reliability, recording noise, or acquisition cost. The corresponding masking distribution becomes modality-specific:

$$p_{\text{IMR}}(e) = \frac{\prod_{m=1}^M (1 - r_m)^{e^m} r_m^{1-e^m}}{1 - \prod_{m=1}^M r_m}, \quad (3)$$

where  $p_{\text{IMR}}(e)$  and  $p_{\text{SMR}}(e)$  denote the probability of observing a particular masking pattern  $e$  under IMR and SMR, respectively. Unlike the homogeneous  $p_{\text{SMR}}$ , the heterogeneous  $p_{\text{IMR}}$  assigns higher probability mass to combinations retaining low- $r_m$  modalities. The degree of imbalance can be quantified by a divergence:

$$\Delta_{\text{IMR}} = \mathcal{D}(p_{\text{IMR}}(e) \parallel p_{\text{SMR}}(e)), \quad (4)$$

where  $\mathcal{D}(\cdot \parallel \cdot)$  is a distributional divergence measure, e.g., KL or Jensen–Shannon distance. A larger  $\Delta_{\text{IMR}}$  reflects stronger modality heterogeneity and sampling bias.

**From Distributional to Learning Imbalance.** The heterogeneous masking distribution  $p_{\text{IMR}}$  induces a persistent *distributional shift* between the training data distribution  $\mathbb{P}_{\text{train}}(\tilde{x}, y)$  and the full-modality distribution  $\mathbb{P}_{\text{full}}(x, y)$ , whose magnitude scales with  $\Delta_{\text{IMR}}$ . This imbalance further propagates to the optimization process. Given a backbone model  $\mathcal{F}$  that produces prediction  $\hat{y}_i = \mathcal{F}(\tilde{x}_i)$ , the learning objective under IMR can be formulated as:

$$\mathcal{L}_{\text{IMR}} = \mathbb{E}_{(\tilde{X}, Y) \sim P_{\text{IMR}}} \left[ \sum_{m=1}^M (1 - r_m) \ell(f_m(\tilde{X}_m), Y) \right], \quad (5)$$

where  $\ell$  denotes the task loss for modality branch  $m$ . The gradient contribution of each modality scales with its availability ratio  $(1 - r_m)$  is computed via:

$$\frac{\partial \mathcal{L}_{\text{IMR}}}{\partial \theta_m} \propto (1 - r_m) \mathbb{E} \left[ \frac{\partial \ell(f_m(\tilde{X}_m), Y)}{\partial \theta_m} \right]. \quad (6)$$

Consequently, modalities with higher missing ratios receive weaker supervision and converge more slowly, resulting in **representation underfitting** and **optimization dominance** by low-missing-rate modalities. (See more in Suppl.B)

**Motivation.** The above analysis reveals two coupled challenges under IMR: (1) *uneven exposure leading to in-*

consistent intra-modal representations, and (2) gradient-level inequality during optimization. To address these issues, we propose a model-agnostic framework that performs rebalancing at both the representation and optimization levels, as illustrated in Fig. 3.

### 3.2. Representation-level Rebalancing with Feature Calibration Module

IMR introduces an imbalanced exposure pattern, where some modalities are observed far more often than others. This imbalance distorts the corresponding unimodal representations, weakening their semantic consistency and compromising cross-modal learning [34]. Here, we introduce **Feature Calibration Module (FCM)** to align modality-specific features that are distorted by uneven exposure under IMR. Instead of imputing missing signals, it leverages global contextual cues aggregated from available modalities to recalibrate unimodal embeddings.

**Feature aggregation under IMR.** Following [16], we obtain modality-wise descriptors to represent the overall statistics of available features. Given the masked features  $\tilde{x}_i^m$  and binary indicators  $e_i^m$  from the masking operator  $\mathcal{M}(x; \mathbf{r})$ , the unimodal global descriptor is computed by averaging available features:

$$x_{glob}^m = \frac{\sum_{i=1}^N \tilde{x}_i^m}{\varepsilon + \sum_{i=1}^N e_i^m}, \quad (7)$$

where  $x_{glob}^m \in \mathbb{R}^{d_m}$  and  $\varepsilon$  is a smoothing hyper-parameter.

**Cross-modal context extraction.** The unimodal descriptors are concatenated and passed through a fully connected layer to capture shared cross-modal context:

$$x_{global} = \text{ReLU}(\mathbf{F}_{global}([x_{glob}^{m_1}, x_{glob}^{m_2}, \dots, x_{glob}^{m_M}])), \quad (8)$$

where  $x_{global} \in \mathbb{R}^{d_{global}}$  encodes the global information jointly derived from all available modalities  $\{m_j\}$ . This representation is then projected to modality-specific calibration weights through independent fully connected layers:

$$w_{cal}^m = \mathbf{F}_{cal}^m(x_{global}), \quad (9)$$

where  $w_{cal}^m \in \mathbb{R}^{d_m}$  represents the contextual calibration weight for modality  $m$ .

**Feature calibration.** Each modality feature is adaptively recalibrated through excitation-based calibration weights derived from global contextual information [12]. These weights highlight the importance of each modality and help correct representation bias under IMR. Formally, a gating operation with sigmoid activation is applied to rescale each unimodal feature:

$$\hat{x}_i^m = (1 + \sigma(w_{cal}^m)) \odot \tilde{x}_i^m, \quad (10)$$

where  $\hat{x}_i^m \in \mathbb{R}^{d_m}$ ,  $\odot$  and  $\sigma(\cdot)$  denote element-wise multiplication and sigmoid function, respectively. Features of missing modalities remain as  $\vec{0}$ .

Although the recalibrated features  $\hat{x}_i^m$  differ in composition, they preserve dimensionality and seamlessly integrated into any backbone. This shared calibration mitigates IMR-induced representation discrepancies and provides a consistent feature basis for downstream optimization.

### 3.3. Model-Agnostic Integration of Multimodal Emotion Recognition Backbone

For compatibility with existing Multimodal Emotion Recognition (MER) frameworks, we keep this stage unchanged. Each sample in MER corresponds to an utterance  $u_i$  with multimodal inputs  $\tilde{x}_i = \{\tilde{x}_i^a, \tilde{x}_i^v, \tilde{x}_i^l\}$  and an emotion label  $y_i \in \mathcal{Y}$ , where  $a, v, l$  denote acoustic, visual, lexical modalities, respectively. The model predicts  $\hat{y}_i$  representing the probability distribution over classes. Our plug-in modules work seamlessly with any backbone, treating missing modalities as  $\vec{0}$  during training and inference.

**Unimodal encoding.** Each modality feature  $\hat{x}_i^m$  from the Feature Calibration Module (FCM) is processed by a modality-specific encoder to obtain semantic embeddings:

$$z_i^m = \phi^m(\hat{x}_i^m), \quad (11)$$

where  $z_i^m \in \mathbb{R}^{d_{emb}}$  denotes the embedding of modality  $m$ , and  $\phi^m(\cdot)$  represents its encoder<sup>1</sup>.

**Multimodal fusion.** The resulting unimodal embeddings are then combined through a fusion network:

$$h_i = \mathcal{F}([z_i^a, z_i^v, z_i^l]), \quad (12)$$

where  $h_i \in \mathbb{R}^{d_h}$  is the fused multimodal representation, and  $\mathcal{F}(\cdot)$  denotes the fusion function<sup>2</sup>.

**Prediction layer.** The fused representation is mapped to the output space through a fully connected prediction head followed by a softmax layer:

$$\hat{y}_i = \delta(\mathbf{F}_{pred}(h_i)), \quad (13)$$

where  $\hat{y}_i \in \mathbb{R}^{|\mathcal{Y}|}$  is the predicted class probability distribution and  $\delta(\cdot)$  denotes the softmax operator.

**Optimization objective.** A task-specific loss  $\ell(\cdot)$ , typically Cross-Entropy or L1, is employed to measure the discrepancy between the predicted and ground-truth labels:

$$\mathcal{L}_{task} = \sum_{i=1}^N \ell(\hat{y}_i, y_i), \quad (14)$$

where  $N$  is the number of utterances in a mini-batch. This loss is used to optimize the parameters of the backbone via gradient-based updates:

$$\theta_{(t+1)} = \theta_{(t)} - \alpha \frac{\partial \mathcal{L}_{task}}{\partial \theta}, \quad (15)$$

where  $\theta$  denotes the model parameters,  $t$  is the current training iteration, and  $\alpha$  is the learning rate.

<sup>1</sup>In practice,  $\phi^m(\cdot)$  is typically implemented using an LSTM, GRU, or multilayer perceptron (MLP) depending on the modality type.

<sup>2</sup> $\mathcal{F}(\cdot)$  can take forms such as concatenation, attention, tensor fusion, or graph-based aggregation, depending on the backbone architecture.

### 3.4. Optimization-level Rebalancing with Gradient Rebalancing Module

Generally, popular modalities drive most gradient updates, resulting in skewed convergence [8]. Here, we propose **Gradient Rebalancing Module (GRM)** to balance learning dynamics across modalities, in which each modality-specific component receives fair and consistent supervision under IMR. We use the latest unimodal embeddings as optimization targets, while their encoders act as modality-specific components.

**Unimodal Prediction Heads.** To quantify optimization discrepancies among modalities, we introduce lightweight unimodal prediction heads that operate independently. Each head consists of two fully connected layers applied to the embeddings from Eq. 11. The first layer projects the embedding dimension to that of the multimodal representation in Eq. 12, followed by a ReLU activation as follows:

$$h_i^m = \text{ReLU}(\mathbf{F}_{map}^m(z_i^m)), \quad (16)$$

where  $h_i^m \in \mathbb{R}^{d_h}$ . The second layer produces modality-specific predictions using the same formulation as Eq. 13:

$$\hat{y}_i^m = \delta(\mathbf{F}_{pred}^m(h_i^m)), \quad (17)$$

where  $\hat{y}_i^m \in \mathbb{R}^{|\mathcal{Y}|}$  and  $\delta(\cdot)$  denotes the softmax operator. We deliberately design these two-layer classifiers to ensure that the gradient matrices of all modality-specific prediction layers  $\mathbf{F}_{pred}^m$  share the same shape ( $d_h \times |\mathcal{Y}|$ ) as the framework’s main prediction layer  $\mathbf{F}_{pred}$ . Each unimodal head is optimized using the same loss function  $\ell(\cdot)$  as in Eq. 14, where the task-specific loss for modality  $m$  is:

$$\mathcal{L}_{task}^m = \sum_{i=1}^N \ell(\hat{y}_i^m, y_i), \quad \theta_{(t+1)}^m = \theta_{(t)}^m - \alpha \frac{\partial \mathcal{L}_{task}^m}{\partial \theta^m}. \quad (18)$$

where  $\theta^m$  is updated via standard gradient descent.

**Gradient Rebalancing Module (GRM).** This module mitigates the optimization bias introduced by imbalanced missing modalities. It adjusts gradient updates of modality-specific encoders from two complementary perspectives: *distribution-driven* and *spatial-driven*.

**Distribution-driven modulation.** Since complete unimodal distributions are unobservable under IMR, modality contributions become skewed as dominant modalities overshadow weaker ones. We therefore approximate the multimodal prediction distribution as a stable reference capturing intra- and inter-modal information. To measure the discrepancy between unimodal predictions and the multimodal reference, we use the Kullback–Leibler (KL) divergence as:

$$\mathcal{D}_{KL}^m = \sum_{i=1}^N \mathbf{KL}(\hat{y}_i^m \parallel \hat{y}_i), \quad (19)$$

where  $\hat{y}_i$  and  $\hat{y}_i^m$  denote the multimodal and unimodal predicted class probability distribution from Eq. 13 and Eq. 17, respectively. A larger  $\mathcal{D}_{KL}^m$  indicates slower convergence of modality  $m$  toward the shared multimodal distribution.

Absolute divergence values are insufficient for tracking learning dynamics, as dominant modalities stabilize quickly while others fluctuate. We thus compute the *relative learning progress* of each modality from the change in divergence between consecutive iterations:

$$\Delta_{KL}^m = \begin{cases} \mathcal{D}_{KL}^{m(t)}, & t = 0, \\ \mathcal{D}_{KL}^{m(t-1)} - \mathcal{D}_{KL}^{m(t)}, & \text{otherwise,} \end{cases} \quad (20)$$

A larger  $\Delta_{KL}^m$  indicates faster alignment with the multimodal reference. Based on these progress signals, we define a *modulation coefficient* for each modality:

$$\mu^m = \rho \frac{\sum_{m' \in \{a,v,l\}, m' \neq m} \Delta_{KL}^{m'}}{\sum_{m' \in \{a,v,l\}} \Delta_{KL}^{m'}}, \quad (21)$$

where  $\rho$  is a saturation hyperparameter controlling the modulation intensity. A smaller  $\mu^m$  indicates that modality  $m$  is learning faster (larger  $\Delta_{KL}^m$ ), and thus its gradient update should be attenuated; conversely, slower modalities receive stronger updates. Accordingly, the parameters of unimodal encoders are updated as:

$$\theta_{(t+1)}^{\phi^m} = \theta_{(t)}^{\phi^m} - \alpha \mu^m \frac{\partial \mathcal{L}_{task}}{\partial \theta_{(t)}^{\phi^m}}, \quad (22)$$

where  $\theta^{\phi^m}$  denotes the parameters of encoder  $\phi^m$ .

**Spatial-driven modulation.** Previous work [38, 45, 54] shows that multimodal optimization follows the dominant modality. This imbalance worsens under missing modalities, so we reorient gradients toward a balanced multimodal direction to stabilize training. Directly computing full unimodal gradients is computationally expensive, and comparing them against the entire model’s gradients is often infeasible. Following [8], we approximate the overall model and modality-specific gradients using those of the multimodal and unimodal prediction heads, respectively:

$$\nabla_{pred} = \nabla_{\theta^{\mathbf{F}_{pred}}} \mathcal{L}_{task} = \frac{\partial \mathcal{L}_{task}}{\partial \theta^{\mathbf{F}_{pred}}}, \quad (23)$$

$$\nabla_{pred}^m = \nabla_{\theta^{\mathbf{F}_{pred}^m}} \mathcal{L}_{task}^m = \frac{\partial \mathcal{L}_{task}^m}{\partial \theta^{\mathbf{F}_{pred}^m}}, \quad (24)$$

where  $\nabla_{pred}$  represents the gradient of the main multimodal classifier and  $\nabla_{pred}^m$  corresponds to the gradient of modality  $m$ ’s prediction head. We measure the spatial discrepancy between these gradients via cosine similarity:

$$\mathcal{D}_{cos}^m = \cos_{sim}(\nabla_{pred}^m, \nabla_{pred}), \quad (25)$$

A lower cosine similarity indicates that modality  $m$  is optimized in a direction less aligned with the multimodal objective. To avoid over-constraint, we adopt a soft spatial

Table 1. Performance on IEMOCAP under different IMR configurations.

Model	(0.3,0.5,0.7)		(0.3,0.7,0.5)		(0.5,0.3,0.7)		(0.5,0.7,0.3)		(0.7,0.3,0.5)		(0.7,0.5,0.3)	
	Acc.	w-F1										
<i>Group 1 (Models addressing missing or imbalanced modalities)</i>												
MMIN [56]	55.97	49.92	55.87	49.83	56.40	50.28	55.87	49.75	55.87	49.85	55.83	49.73
SDR-GNN [7]	59.46	59.34	54.16	53.59	58.53	58.42	56.56	56.77	55.14	55.22	55.45	55.17
Mi-CGA [28]	58.84	58.80	54.65	54.61	60.50	60.25	56.19	56.11	58.84	58.63	58.72	58.22
MoMKE [50]	55.39	54.19	50.83	49.70	60.18	59.94	50.77	50.15	58.26	58.45	54.78	54.92
GCNet [19]	58.04	58.36	56.81	56.83	61.61	62.06	56.81	56.99	59.64	59.78	59.09	59.19
Ada2I [27]	61.98	60.68	61.98	61.46	61.37	60.45	58.10	58.22	61.74	60.90	57.73	54.76
RedCore [34]	46.27	46.32	43.38	43.40	50.15	47.92	43.69	43.60	50.59	50.53	46.09	46.21
MCE [55]	46.52	45.54	44.36	43.48	50.65	49.22	42.64	41.70	50.34	49.45	44.73	44.40
<b>GCNet<sub>+BALM</sub></b>	<b>61.31<math>\pm</math>0.75</b>	<b>61.33<math>\pm</math>0.70</b>	<b>57.36<math>\pm</math>0.76</b>	<b>57.00<math>\pm</math>0.83</b>	<b>61.31<math>\pm</math>0.63</b>	<b>61.62<math>\pm</math>0.59</b>	<b>57.64<math>\pm</math>1.10</b>	<b>57.64<math>\pm</math>1.22</b>	<b>59.33<math>\pm</math>0.46</b>	<b>59.39<math>\pm</math>0.50</b>	<b>60.26<math>\pm</math>0.83</b>	<b>60.58<math>\pm</math>0.96</b>
$\Delta$ (vs origin GCNet)	+3.27	+2.97	+0.55	+0.17	-0.30	-0.44	+0.83	+0.65	-0.31	-0.39	+1.17	+1.39
$\Delta_1$ (vs Grp1 mean)	+6.00	+7.19	+4.61	+5.39	+4.21	+5.55	+5.06	+5.98	+3.03	+4.04	+6.21	+7.76
<i>Group 2 (Typical MER Models)</i>												
MMGCN [13]	63.59	63.62	59.09	58.99	64.63	64.95	57.79	57.99	64.14	64.27	60.63	60.85
<b>MMGCN<sub>+BALM</sub></b>	<b>64.39<math>\pm</math>0.88</b>	<b>63.82<math>\pm</math>0.89</b>	<b>60.07<math>\pm</math>0.70</b>	<b>60.04<math>\pm</math>0.65</b>	<b>65.37<math>\pm</math>0.61</b>	<b>65.03<math>\pm</math>0.63</b>	<b>62.29<math>\pm</math>0.75</b>	<b>62.35<math>\pm</math>0.70</b>	<b>65.00<math>\pm</math>1.54</b>	<b>64.98<math>\pm</math>1.77</b>	<b>61.74<math>\pm</math>0.96</b>	<b>61.20<math>\pm</math>0.82</b>
$\Delta$ (vs origin MMGCN)	+0.80	+0.20	+0.98	+1.05	+0.74	+0.08	+4.50	+4.36	+0.86	+0.71	+1.11	+0.35
$\Delta_1$ (vs Group1 mean)	+9.08	+9.68	+7.32	+8.43	+7.95	+8.96	+9.71	+10.69	+8.70	+9.63	+7.69	+8.38
MMDFN [11]	63.34	63.00	60.38	60.01	67.34	67.40	57.92	56.25	66.48	66.67	63.65	64.00
<b>MMDFN<sub>+BALM</sub></b>	<b>67.34<math>\pm</math>0.84</b>	<b>66.64<math>\pm</math>0.94</b>	<b>63.40<math>\pm</math>0.45</b>	<b>63.11<math>\pm</math>0.47</b>	<b>68.76<math>\pm</math>0.22</b>	<b>68.25<math>\pm</math>0.18</b>	<b>64.02<math>\pm</math>1.11</b>	<b>63.76<math>\pm</math>1.05</b>	<b>67.22<math>\pm</math>1.03</b>	<b>67.02<math>\pm</math>1.06</b>	<b>65.50<math>\pm</math>0.47</b>	<b>64.98<math>\pm</math>0.64</b>
$\Delta$ (vs origin MMDFN)	+4.00	+3.64	+3.02	+3.10	+1.42	+0.85	+6.10	+7.51	+0.74	+0.35	+1.85	+0.98
$\Delta_1$ (vs Group1 mean)	+12.03	+12.50	+10.65	+11.50	+11.34	+12.18	+11.44	+12.10	+10.92	+11.67	+11.45	+12.16

Note. ( $r_A, r_L, r_V$ ) denotes the missing rates for Audio, Language, and Visual modalities.  $\Delta$  and  $\Delta_1$  denote performance differences relative to the original backbone and mean of Group 1 models, respectively.

alignment strategy, which minimizes the weighted absolute deviation of cosine similarities:

$$\mathcal{L}_{mod} = \sum_{m \in \{a,v,l\}} |\mathcal{D}_{cos}^m \times \mu^m|, \quad (26)$$

where  $\mu^m$  are dynamic modulation coefficients from Eq. 21, adaptively weighting each modality’s contribution during spatial alignment under IMR.

**Overall Objective.** The overall training objective integrates the task loss and the modulation loss as:

$$\mathcal{L} = \mathcal{L}_{task} + \tau \mathcal{L}_{mod}, \quad (27)$$

where  $\tau$  is a trade-off hyperparameter.

The modality-specific classifiers introduced in Sec. 3.4 are optimized independently using  $\mathcal{L}_{task}^m$  as auxiliary objectives and are therefore excluded from Eq. 27. The complete training procedure is summarized in Suppl. A.

## 4. Experiments

### 4.1. Experimental Settings

**Datasets and Evaluation Metrics.** We conduct experiments on two multimodal emotion recognition datasets: **IEMOCAP** [3] (6-way) and **CMU-MOSEI** [52], each containing audio (A), visual (V), and lexical (L) modalities. We adopt Accuracy (Acc.) and Weighted F1-score (w-F1) as evaluation metrics to assess model performance.

**Baselines.** We evaluate BALM with two main groups of baselines: (1) **Models addressing missing or imbalanced modalities**, including *MMIN* [56], *SDR-GNN* [7],

*Mi-CGA* [28], *MoMKE* [50], and *GCNet* [19] for missing-modality learning; *Ada2I* [27] for modality imbalance; *RedCore* [34] and *MCE* [55] which jointly handles both aspects; and (2) **Typical MER backbones**, *MMGCN* [13] and *MMDFN* [11], representing standard multimodal architectures. All models are trained from scratch, with missing modalities simulated under shared (*SMR*) or imbalanced (*IMR*) rates defined in Sec. 3.1.

Our plug-in (**+BALM**) is integrated without altering backbone architectures and supports both early- and late-fusion setups. This setup enables evaluating BALM across incomplete, imbalanced, and standard MER backbones. Further dataset statistics, baseline descriptions, and implementation details are provided in the Suppl. E.

### 4.2. Main Results

**Performance Comparison.** Tables 1 and 2 present results under different IMR settings with  $(r_A, r_L, r_V) \in \{0.3, 0.5, 0.7\}$ , where integrating **BALM** consistently improves all metrics across all backbones.

As shown in Table 1, integrating BALM consistently boosts both missing-modality and emotion-recognition baselines. For example, GCNet<sub>+BALM</sub> yields a gain of up to +3.27% Acc over the original GCNet on the (0.3, 0.5, 0.7) setting. It consistently outperforms other missing-modality baselines. Under the (0.7, 0.5, 0.3) configuration, it improves w-F1 by roughly +7.0% compared with the *Group 1* mean. These results confirm its effectiveness in reducing bias caused by uneven modality availability. Compared with recent IMR-oriented works of *Group 1*, which explicitly model missing patterns, stronger fusion backbones integrated with BALM, notably MMDFN<sub>+BALM</sub> and

Table 2. Performance on CMU-MOSEI under different IMR configurations.

Model	(0.3, 0.5, 0.7)		(0.3, 0.7, 0.5)		(0.5, 0.3, 0.7)		(0.5, 0.7, 0.3)		(0.7, 0.3, 0.5)		(0.7, 0.5, 0.3)	
	Acc.	w-F1										
<b>Group 1 (Models addressing missing or imbalanced modalities)</b>												
MMIN [56]	75.87	75.52	71.93	71.60	79.72	79.69	71.46	71.30	78.92	78.45	75.65	75.81
SDR-GNN [7]	80.13	80.14	77.38	77.38	83.35	83.03	76.69	76.75	83.54	83.44	81.67	81.21
Mi-CGA [28]	81.04	80.97	77.38	77.11	82.55	82.37	76.42	76.45	82.86	82.64	80.65	80.33
MoMKE [50]	78.43	78.39	74.16	74.19	82.17	81.86	74.38	73.93	82.11	81.79	77.27	76.77
GCNet [19]	81.43	81.07	78.23	78.14	82.64	82.78	78.34	78.51	83.76	83.57	81.45	81.24
Ada2I [27]	82.42	82.28	78.07	77.53	83.82	83.57	77.68	76.97	83.38	83.49	81.87	81.61
RedCore [34]	74.88	72.89	70.51	64.25	75.05	72.82	75.01	72.79	74.37	72.71	74.94	73.59
<b>GCNet<sub>+BALM</sub></b>	<b>81.54<math>\pm</math>0.58</b>	<b>81.40<math>\pm</math>0.59</b>	<b>78.51<math>\pm</math>0.61</b>	<b>78.33<math>\pm</math>0.49</b>	<b>83.27<math>\pm</math>0.26</b>	<b>83.24<math>\pm</math>0.33</b>	<b>79.50<math>\pm</math>0.99</b>	<b>79.22<math>\pm</math>0.84</b>	<b>83.63<math>\pm</math>0.35</b>	<b>83.57<math>\pm</math>0.48</b>	<b>82.09<math>\pm</math>0.75</b>	<b>81.84<math>\pm</math>0.72</b>
$\Delta$ (vs origin GCNet)	+0.11	+0.33	+0.28	+0.19	+0.63	+0.46	+1.16	+0.71	-0.13	+0.00	+0.64	+0.60
$\Delta_1$ (vs Group1 mean)	+2.37	+2.65	+3.13	+4.02	+1.94	+2.37	+3.79	+3.98	+2.35	+2.70	+3.02	+3.19
<b>Group 2 (Typical MER Models)</b>												
MMGCN [13]	80.82	80.20	78.32	77.35	84.76	84.60	78.12	78.17	84.04	84.04	81.54	81.62
<b>MMGCN<sub>+BALM</sub></b>	<b>82.03<math>\pm</math>0.31</b>	<b>81.74<math>\pm</math>0.28</b>	<b>78.73<math>\pm</math>0.27</b>	<b>78.33<math>\pm</math>0.31</b>	<b>84.54<math>\pm</math>0.32</b>	<b>84.34<math>\pm</math>0.29</b>	<b>79.83<math>\pm</math>0.49</b>	<b>79.44<math>\pm</math>0.37</b>	<b>84.84<math>\pm</math>0.29</b>	<b>84.70<math>\pm</math>0.32</b>	<b>82.50<math>\pm</math>0.49</b>	<b>82.36<math>\pm</math>0.54</b>
$\Delta$ (vs origin MMGCN)	+1.21	+1.54	+0.41	+0.98	-0.22	-0.26	+1.71	+1.27	+0.80	+0.66	+0.96	+0.74
$\Delta_1$ (vs Group1 mean)	+2.86	+2.99	+3.35	+4.02	+3.21	+3.47	+4.12	+4.20	+3.56	+3.83	+3.43	+3.71
MMDFN [11]	82.17	81.76	78.37	78.14	84.18	83.92	78.87	79.03	84.37	84.30	81.89	81.69
<b>MMDFN<sub>+BALM</sub></b>	<b>82.06<math>\pm</math>0.43</b>	<b>81.73<math>\pm</math>0.45</b>	<b>78.81<math>\pm</math>0.58</b>	<b>78.50<math>\pm</math>0.63</b>	<b>84.34<math>\pm</math>0.44</b>	<b>84.14<math>\pm</math>0.39</b>	<b>79.36<math>\pm</math>0.39</b>	<b>79.19<math>\pm</math>0.39</b>	<b>84.78<math>\pm</math>0.21</b>	<b>84.68<math>\pm</math>0.26</b>	<b>82.53<math>\pm</math>0.35</b>	<b>82.29<math>\pm</math>0.28</b>
$\Delta$ (vs origin MMDFN)	-0.11	-0.03	+0.44	+0.36	+0.16	+0.22	+0.49	+0.16	+0.41	+0.38	+0.64	+0.60
$\Delta_1$ (vs Group1 mean)	+2.89	+2.98	+3.43	+4.19	+2.63	+3.03	+3.65	+3.95	+3.50	+3.81	+3.46	+3.64

Note. ( $r_A, r_L, r_V$ ) denotes the missing rates for Audio, Language, and Visual modalities.  $\Delta$  and  $\Delta_1$  denote performance differences relative to the original model and the mean of Group 1 models, respectively.

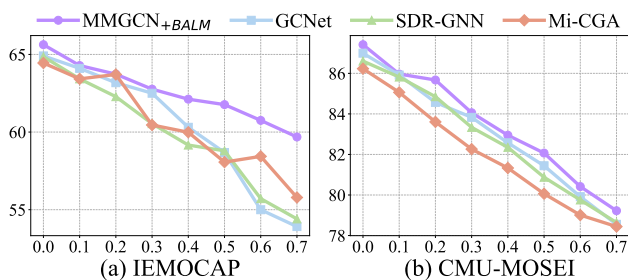


Figure 4. Average accuracy under different SMR settings

MMGCN<sub>+BALM</sub>, achieve even higher performance across different missing scenarios. In addition, BALM elevates both MER models in all missing configurations (up to 7.51% w-F1 gap over the original backbone of MMDFN<sub>+BALM</sub>), and raises their performance lower-bound to above 60% for both Acc and w-F1. These results suggest that rebalancing, representation- and optimization-wise, provides complementary benefits for high-capacity fusion architectures. Ada2I, which addresses imbalance learning for MER, performs better than conventional missing-modality models but still degrades under IMR, showing that gradient balancing alone is insufficient when missingness occurs.

Likewise, on CMU-MOSEI (Table 2), BALM consistently improves performance across IMR settings with smaller but steady gains, reflecting the dataset’s lower modality noise and weaker sensitivity to missing-rate variations. Persistent with the observation in the previous dataset, high language-missing rates in CMU-MOSEI lead to higher performance degradation, and in return, such con-

figurations highlight the effectiveness of BALM in elevating backbones’ performance. Specifically, MMGCN<sub>+BALM</sub> achieves a +1.71% Acc gain over the original MMGCN, widen the gap with *Group 1* mean to +4.12% Acc under (0.5, 0.7, 0.3) setting, a similar boost can also be found on GCNet<sub>+BALM</sub> under the same setting.

For both dataset, moderate to high loss of visual (e.g., (0.7, 0.3, 0.5), (0.5, 0.3, 0.7)) usually leads to lower degradation comparing to other modalities. Whereas, high missing rates in language (e.g., (0.3, 0.7, 0.5)) lead to profound performance drops, confirming that lexical information is the most discriminative yet vulnerable modality. When audio missingness is also high alongside language (e.g., (0.5, 0.7, 0.3)), the degradation becomes more pronounced, underscoring the critical role of robust auditory cues. These divergent behaviors when modalities take turn suffering low/high missing rate, along with the consistent gains of the backbones after integrating with BALM, further validate the need to address modalities’ discrepancy stem from IMR.

**Evaluating Robustness under SMR Settings.** To ensure a fair cross-evaluation, we adopt the same settings and model configurations as in the IMR experiments, while uniformly applying identical missing rates to all modalities (SMR). As shown in Fig. 4, integrating BALM consistently outperforms all baselines under SMR settings,<sup>3</sup> indicating that our approach not only handles the challenging IMR scenario but also maintains superior robustness and generalization under balanced missing conditions.

<sup>3</sup>Each result is averaged over five independent runs with different random seeds for each shared missing rate.

Table 3. Average performance on different modality combinations.

Setting	MMGCN		+FCM	
	Acc	w-F1	Acc	w-F1
IEMOCAP	48.09	44.81	<b>50.99</b> <sub>(±2.90)</sub>	<b>47.62</b> <sub>(±2.81)</sub>
CMU-MOSEI	75.23	69.17	<b>75.97</b> <sub>(±0.74)</sub>	<b>70.09</b> <sub>(±0.92)</sub>

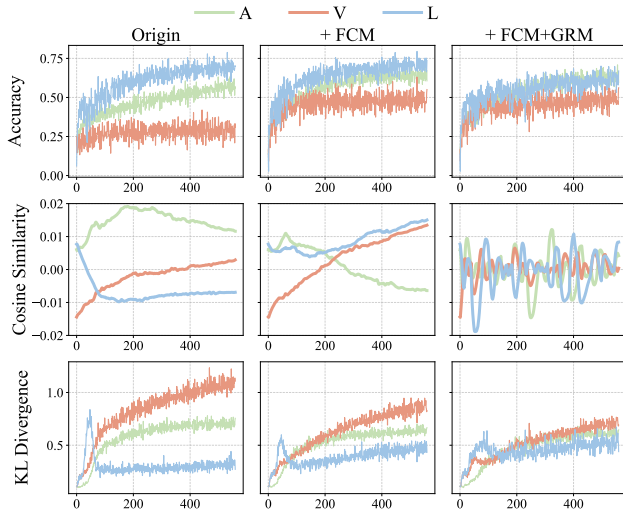


Figure 5. Modality discrepancies on IEMOCAP with MMGCN.

### 4.3. Ablation Study

**Effect of Rebalancing Modules.** Table 3 summarizes the average performance over modality combinations under the IMR setting  $(r_A, r_L, r_V) = (0.5, 0.7, 0.3)$ . FCM consistently improves results on both datasets, boosting w-F1 by +2.81% on IEMOCAP and +0.92% on MOSEI.

As illustrated in Fig. 5, FCM effectively enhances feature-level consistency by reducing representation discrepancies among modalities; however, it does not fully resolve the imbalance in gradient magnitudes across branches. Building on this, GRM further rebalances the gradient flow. In particular, the lexical branch tends to dominate optimization, resulting in large cross-modal divergence. With GRM, the inter-modal cosine similarity increases and the KL divergence stabilizes, indicating that gradient rebalancing harmonizes multimodal optimization and alleviates dominance from high-availability modalities.

**Modality Combination.** Fig. 6 shows that BALM consistently improves both GCNet and MMGCN across most modality combinations on IEMOCAP, with the largest gains on audio and lexical branches (up to +5.3% w-F1). Slight drops in settings where only the visual modality is available stem partly from the low quality of visual cues in IEMOCAP and partly from the fusion architecture of each baseline. Fusion-based methods like MMGCN were originally developed for MER and use modality-specific encoders and

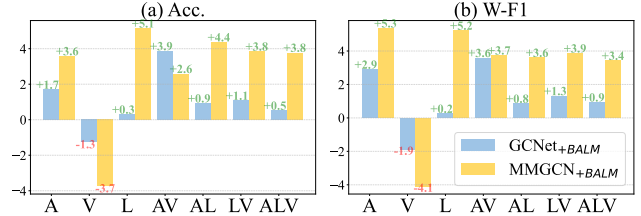


Figure 6. Improvement of GCNet+*BALM* and MMGCN+*BALM* comparing to GCNet on IEMOCAP

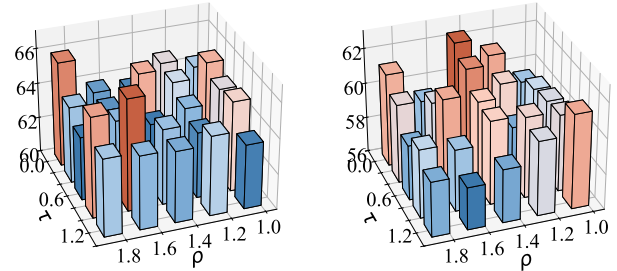


Figure 7. Weighted-F1 sensitivity to hyperparameters under two missing-rate configurations of audio, language and visual.

fusion mechanisms, which makes them more sensitive to variations in modality quality. As a result, they experience larger performance drops. In contrast, GCNet incorporates mechanisms to handle missing modalities and is more alignment-aware, enabling it to capture modality-specific cues and suffer less degradation under the same conditions.

**Hyperparameter Sensitivity under Contrasting Missing Rates.** Fig. 7 compares w-F1 of MMGCN+*BALM* under two contrasting missing-rate settings on IEMOCAP: *Config-A*:  $(0.5, 0.3, 0.7)$  and *Config-B*:  $(0.5, 0.7, 0.3)$ . In *Config-A*, where the least missing-sensitive modality, i.e. visual, is highly missing, w-F1 is stable around 63 – 64% despite the change in  $\tau, \rho$ . Conversely, in *Config-B*, where the more vulnerable modality, i.e. lexical, suffers highest missing rate, the imbalance-aware regularization yields more distinct effectiveness, as higher performance can be achieved with proper selection of  $\rho$  or  $\tau$ . These results underscore the importance of **adaptive regulation** for imbalanced missing-modality scenarios.

**Severe Missing Rate Evaluation.** Table 4 presents the robustness evaluation under extreme missing-modality conditions. As audio and language are informative modalities in MER, their absence typically leads to notable degradation. Nevertheless, BALM consistently stabilizes performance across settings. For instance, when 90% of the language modality is missing, MMGCN+*BALM* achieves a

Table 4. Performance of MMGCN with BALM under severe missing-modality settings, where the arrows indicate the relative change compared to the mean performance of the two baselines.

$(r_A, r_L, r_V)$	Model	IEMOCAP		CMU-MOSEI	
		Acc	w-F1	Acc	w-F1
(0.1, 0.1, 0.9)	GCNet	63.71	63.43	84.62	84.64
	MMGCN	68.02	67.69	85.91	85.52
	MMGCN+BALM	<b>65.87</b> <sub>+0.01</sub>	<b>65.57</b> <sub>+0.01</sub>	<b>85.91</b> <sub>+0.64</sub>	<b>85.70</b> <sub>+0.62</sub>
(0.1, 0.9, 0.1)	GCNet	55.14	55.09	72.15	71.69
	MMGCN	52.74	52.69	71.55	71.70
	MMGCN+BALM	<b>58.72</b> <sub>+4.78</sub>	<b>58.11</b> <sub>+4.22</sub>	<b>72.62</b> <sub>+0.77</sub>	<b>72.15</b> <sub>+0.46</sub>
(0.9, 0.1, 0.1)	GCNet	59.40	58.83	86.24	86.10
	MMGCN	64.82	64.93	86.43	86.42
	MMGCN+BALM	<b>66.24</b> <sub>+4.13</sub>	<b>66.27</b> <sub>+4.39</sub>	<b>86.35</b> <sub>+0.01</sub>	<b>86.38</b> <sub>+0.12</sub>
(0.6, 0.6, 0.9)	GCNet	56.93	56.54	81.81	81.86
	MMGCN	60.63	60.75	81.32	81.16
	MMGCN+BALM	<b>61.74</b> <sub>+2.96</sub>	<b>61.92</b> <sub>+2.28</sub>	<b>81.65</b> <sub>+0.09</sub>	<b>81.62</b> <sub>+0.11</sub>
(0.6, 0.9, 0.6)	GCNet	54.84	54.85	76.00	76.02
	MMGCN	55.64	55.61	76.36	75.97
	MMGCN+BALM	<b>57.30</b> <sub>+2.06</sub>	<b>57.48</b> <sub>+2.25</sub>	<b>76.55</b> <sub>+0.37</sub>	<b>75.30</b> <sub>+0.70</sub>
(0.9, 0.6, 0.6)	GCNet	57.98	58.16	81.45	81.06
	MMGCN	59.95	59.89	81.59	81.50
	MMGCN+BALM	<b>61.68</b> <sub>+2.72</sub>	<b>61.63</b> <sub>+2.61</sub>	<b>82.00</b> <sub>+0.48</sub>	<b>81.55</b> <sub>+0.27</sub>

+4.78% accuracy gain on IEMOCAP compared to the mean of baselines (eg. GCNet, MMGCN). Under heavy audio missing (0.9, 0.6, 0.6), it still improves by +2.72% on accuracy. Although a few settings exhibit minor performance drops, the overall trend indicates BALM effectively mitigates imbalance effects and maintains robustness even when informative modalities are severely incomplete.

## 5. Conclusion

This paper presents BALM, a lightweight and model-agnostic framework for multimodal learning under imbalanced missing conditions. By combining the Feature Calibration Module (FCM) and Gradient Rebalancing Module (GRM), BALM effectively mitigates both representation and optimization imbalance. Extensive experiments on multiple MER backbones demonstrate that BALM consistently improves performance across standard, incomplete, and imbalanced-modality settings. The results highlight its robustness to heterogeneous missing patterns and its ability to maintain stable optimization even when modality availability varies significantly. Future work will explore broader multimodal tasks and large-scale pretrained backbones.

## References

- [1] Galen Andrew, Raman Arora, Jeff Bilmes, and Karen Livescu. Deep canonical correlation analysis. In *International conference on machine learning*, pages 1247–1255. PMLR, 2013. 2
- [2] Tadas Baltrušaitis, Chaitanya Ahuja, and Louis-Philippe Morency. Multimodal machine learning: A survey and taxonomy. *IEEE transactions on pattern analysis and machine intelligence*, 41(2):423–443, 2018. 1
- [3] Carlos Busso, Murtaza Bulut, Chi-Chun Lee, Abe Kazemzadeh, Emily Mower, Samuel Kim, Jean-

nette N Chang, Sungbok Lee, and Shrikanth S Narayanan. Iemocap: Interactive emotional dyadic motion capture database. *Language resources and evaluation*, 42:335–359, 2008. 6, 2

- [4] Ruiting Dai, Chenxi Li, Yandong Yan, Lisi Mo, Ke Qin, and Tao He. Unbiased missing-modality multimodal learning. In *Proceedings of the IEEE/CVF International Conference on Computer Vision*, pages 24507–24517, 2025. 2
- [5] Ruiting Dai, Wenwei Zhu, Zheyu Wang, Haoran Meng, Zhengdao Yuan, Yandong Yan, and Lisi Mo.  $\gamma$ -crd: Gamma-cooperative retrieval diffusion model for robust incomplete multimodal learning. In *Proceedings of the 2025 International Conference on Multimedia Retrieval*, pages 173–182, 2025. 2
- [6] Florian Eyben, Felix Weninger, Florian Gross, and Björn Schuller. Recent developments in opensmile, the munich open-source multimedia feature extractor. In *Proceedings of the 21st ACM international conference on Multimedia*, pages 835–838, 2013. 2
- [7] Fangze Fu, Wei Ai, Fan Yang, Yuntao Shou, Tao Meng, and Keqin Li. Sdr-gnn: Spectral domain reconstruction graph neural network for incomplete multimodal learning in conversational emotion recognition. *Knowledge-Based Systems*, page 112825, 2024. 2, 6, 7, 3
- [8] Zirun Guo, Tao Jin, Jingyuan Chen, and Zhou Zhao. Classifier-guided gradient modulation for enhanced multimodal learning. *Advances in Neural Information Processing Systems*, 37:133328–133344, 2024. 2, 5
- [9] Pengcheng He, Xiaodong Liu, Jianfeng Gao, and Weizhu Chen. DeBERTa: Decoding-enhanced bert with disentangled attention. *arXiv preprint arXiv:2006.03654*, 2020. 3
- [10] Harold Hotelling. Relations between two sets of variates. In *Breakthroughs in statistics: methodology and distribution*, pages 162–190. Springer, 1992. 2
- [11] Dou Hu, Xiaolong Hou, Lingwei Wei, Lianxin Jiang, and Yang Mo. Mm-dfn: Multimodal dynamic fusion network for emotion recognition in conversations. In *ICASSP 2022-2022 IEEE International Conference on Acoustics, Speech and Signal Processing (ICASSP)*, pages 7037–7041. IEEE, 2022. 6, 7, 2, 3
- [12] Jie Hu, Li Shen, and Gang Sun. Squeeze-and-excitation networks. In *Proceedings of the IEEE conference on computer vision and pattern recognition*, pages 7132–7141, 2018. 4
- [13] Jingwen Hu, Yuchen Liu, Jinming Zhao, and Qin Jin. MMGCN: Multimodal fusion via deep graph convolution network for emotion recognition in conversation. In *Proceedings of the 59th Annual Meeting of the Association for Computational Linguistics and the*

- 11th International Joint Conference on Natural Language Processing (Volume 1: Long Papers)*, pages 5666–5675, Online, 2021. Association for Computational Linguistics. 6, 7, 2, 3
- [14] Cong Hua, Qianqian Xu, Shilong Bao, Zhiyong Yang, and Qingming Huang. Reconboost: boosting can achieve modality reconciliation. In *Proceedings of the 41st International Conference on Machine Learning*, pages 19573–19597, 2024. 2
- [15] Gao Huang, Zhuang Liu, Laurens Van Der Maaten, and Kilian Q Weinberger. Densely connected convolutional networks. In *Proceedings of the IEEE conference on computer vision and pattern recognition*, pages 4700–4708, 2017. 2
- [16] Yewon Hwang and Jong-Hwan Kim. Self-supervised unimodal label generation strategy using recalibrated modality representations for multimodal sentiment analysis. In *Findings of the Association for Computational Linguistics: EACL 2023*, pages 35–46, 2023. 4
- [17] Hong Li, Xingyu Li, Pengbo Hu, Yinuo Lei, Chunxiao Li, and Yi Zhou. Boosting multi-modal model performance with adaptive gradient modulation. In *Proceedings of the IEEE/CVF International Conference on Computer Vision*, pages 22214–22224, 2023. 2
- [18] Mingcheng Li, Dingkan Yang, Xiao Zhao, Shuaibing Wang, Yan Wang, Kun Yang, Mingyang Sun, Dongliang Kou, Ziyun Qian, and Lihua Zhang. Correlation-decoupled knowledge distillation for multimodal sentiment analysis with incomplete modalities. In *Proceedings of the IEEE/CVF Conference on Computer Vision and Pattern Recognition*, pages 12458–12468, 2024. 2
- [19] Zheng Lian, Lan Chen, Licai Sun, Bin Liu, and Jianhua Tao. Gcnet: Graph completion network for incomplete multimodal learning in conversation. *IEEE Transactions on Pattern Analysis and Machine Intelligence*, 2023. 1, 2, 6, 7, 3
- [20] Paul Pu Liang, Amir Zadeh, and Louis-Philippe Morency. Foundations & trends in multimodal machine learning: Principles, challenges, and open questions. *ACM Computing Surveys*, 56(10):1–42, 2024. 1
- [21] Ronghao Lin, Qiaolin He, Sijie Mai, Ying Zeng, Aolin Xiong, Li Huang, Yap-Peng Tan, and Haifeng Hu. Cyin: Cyclic informative latent space for bridging complete and incomplete multimodal learning. In *The Thirty-ninth Annual Conference on Neural Information Processing Systems*, 2025. 1
- [22] Rui Liu, Haolin Zuo, Zheng Lian, Björn W Schuller, and Haizhou Li. Contrastive learning based modality-invariant feature acquisition for robust multimodal emotion recognition with missing modalities. *IEEE Transactions on Affective Computing*, 15(4):1856–1873, 2024. 1, 2
- [23] Yinhan Liu, Myle Ott, Naman Goyal, Jingfei Du, Mandar Joshi, Danqi Chen, Omer Levy, Mike Lewis, Luke Zettlemoyer, and Veselin Stoyanov. Roberta: A robustly optimized bert pretraining approach. *arXiv preprint arXiv:1907.11692*, 2019. 2
- [24] Huan Ma, Qingyang Zhang, Changqing Zhang, Bingzhe Wu, Huazhu Fu, Joey Tianyi Zhou, and Qinghua Hu. Calibrating multimodal learning. In *International Conference on Machine Learning*, pages 23429–23450. PMLR, 2023. 2
- [25] Hui Ma, Jian Wang, Hongfei Lin, Bo Zhang, Yijia Zhang, and Bo Xu. A transformer-based model with self-distillation for multimodal emotion recognition in conversations. *IEEE Transactions on Multimedia*, 26: 776–788, 2024. 2
- [26] Mengmeng Ma, Jian Ren, Long Zhao, Sergey Tulyakov, Cathy Wu, and Xi Peng. Smil: Multimodal learning with severely missing modality. In *Proceedings of the AAAI Conference on Artificial Intelligence*, pages 2302–2310, 2021. 1, 2
- [27] Cam-Van Thi Nguyen, The-Son Le, Anh-Tuan Mai, and Duc-Trong Le. Ada2i: Enhancing modality balance for multimodal conversational emotion recognition. In *Proceedings of the 32nd ACM International Conference on Multimedia*, pages 9330–9339, 2024. 2, 6, 7, 3
- [28] Cam-Van Thi Nguyen, Hai-Dang Kieu, Quang-Thuy Ha, Xuan-Hieu Phan, and Duc-Trong Le. Mi-cga: Cross-modal graph attention network for robust emotion recognition in the presence of incomplete modalities. *Neurocomputing*, 623:129342, 2025. 1, 2, 6, 7, 3
- [29] Xiaokang Peng, Yake Wei, Andong Deng, Dong Wang, and Di Hu. Balanced multimodal learning via on-the-fly gradient modulation. In *Proceedings of the IEEE/CVF conference on computer vision and pattern recognition*, pages 8238–8247, 2022. 2
- [30] Hai Pham, Paul Pu Liang, Thomas Manzini, Louis-Philippe Morency, and Barnabás Póczos. Found in translation: Learning robust joint representations by cyclic translations between modalities. In *Proceedings of the AAAI Conference on Artificial Intelligence*, pages 6892–6899, 2019. 1, 2
- [31] Soujanya Poria, Erik Cambria, Rajiv Bajpai, and Amir Hussain. A review of affective computing: From unimodal analysis to multimodal fusion. *Information fusion*, 37:98–125, 2017. 1
- [32] Steffen Schneider, Alexei Baevski, Ronan Collobert, and Michael Auli. wav2vec: Unsupervised pre-training for speech recognition. *arXiv preprint arXiv:1904.05862*, 2019. 2

- [33] Junjie Shi, Caozhi Shang, Zhaobin Sun, Li Yu, Xin Yang, and Zengqiang Yan. Passion: Towards effective incomplete multi-modal medical image segmentation with imbalanced missing rates. In *Proceedings of the 32nd ACM International Conference on Multimedia*, pages 456–465, 2024. 2
- [34] Jun Sun, Xinxin Zhang, Shoukang Han, Yu-Ping Ruan, and Taihao Li. Redcore: Relative advantage aware cross-modal representation learning for missing modalities with imbalanced missing rates. In *Proceedings of the AAAI Conference on Artificial Intelligence*, pages 15173–15182, 2024. 2, 4, 6, 7, 3
- [35] Luan Tran, Xiaoming Liu, Jiayu Zhou, and Rong Jin. Missing modalities imputation via cascaded residual autoencoder. In *Proceedings of the IEEE conference on computer vision and pattern recognition*, pages 1405–1414, 2017. 2
- [36] Yao-Hung Hubert Tsai, Shaojie Bai, Paul Pu Liang, J Zico Kolter, Louis-Philippe Morency, and Ruslan Salakhutdinov. Multimodal transformer for unaligned multimodal language sequences. In *Proceedings of the conference. Association for computational linguistics. Meeting*, page 6558, 2019. 2
- [37] Weiran Wang, Raman Arora, Karen Livescu, and Jeff Bilmes. On deep multi-view representation learning. In *International conference on machine learning*, pages 1083–1092. PMLR, 2015. 2
- [38] Weiyao Wang, Du Tran, and Matt Feiszli. What makes training multi-modal classification networks hard? In *Proceedings of the IEEE/CVF conference on computer vision and pattern recognition*, pages 12695–12705, 2020. 1, 2, 5
- [39] Yuanzhi Wang, Zhen Cui, and Yong Li. Distribution-consistent modal recovering for incomplete multimodal learning. In *Proceedings of the IEEE/CVF International Conference on Computer Vision*, pages 22025–22034, 2023. 2
- [40] Yuanzhi Wang, Yong Li, and Zhen Cui. Incomplete multimodality-diffused emotion recognition. *Advances in Neural Information Processing Systems*, 36: 17117–17128, 2023. 1
- [41] Yuanzhi Wang, Yong Li, and Zhen Cui. Incomplete multimodality-diffused emotion recognition. *Advances in Neural Information Processing Systems*, 36, 2024. 2
- [42] Yake Wei and Di Hu. Mmpareto: Boosting multimodal learning with innocent unimodal assistance. In *International Conference on Machine Learning*, pages 52559–52572. PMLR, 2024. 2
- [43] Yake Wei, Ruoxuan Feng, Ziheng Wang, and Di Hu. Enhancing multimodal cooperation via sample-level modality valuation. In *Proceedings of the IEEE/CVF Conference on Computer Vision and Pattern Recognition*, pages 27338–27347, 2024. 2
- [44] Yake Wei, Siwei Li, Ruoxuan Feng, and Di Hu. Diagnosing and re-learning for balanced multimodal learning. In *European Conference on Computer Vision*, pages 71–86. Springer, 2024. 2
- [45] Nan Wu, Stanislaw Jastrzebski, Kyunghyun Cho, and Krzysztof J Geras. Characterizing and overcoming the greedy nature of learning in multi-modal deep neural networks. In *International Conference on Machine Learning*, pages 24043–24055. PMLR, 2022. 1, 2, 5
- [46] Renjie Wu, Hu Wang, Hsiang-Ting Chen, and Gustavo Carneiro. Deep multimodal learning with missing modality: A survey. *arXiv preprint arXiv:2409.07825*, 2024. 1
- [47] Peng Xu, Xiatian Zhu, and David A Clifton. Multimodal learning with transformers: A survey. *IEEE Transactions on Pattern Analysis and Machine Intelligence*, 45(10):12113–12132, 2023. 1
- [48] Ruize Xu, Ruoxuan Feng, Shi-Xiong Zhang, and Di Hu. Mmcosine: Multi-modal cosine loss towards balanced audio-visual fine-grained learning. In *ICASSP 2023-2023 IEEE International Conference on Acoustics, Speech and Signal Processing (ICASSP)*, pages 1–5. IEEE, 2023. 2
- [49] Shaoxuan Xu, Menglu Cui, Chengxiang Huang, Hongfa Wang, and Di Hu. Balancebenchmark: A survey for multimodal imbalance learning. *arXiv preprint arXiv:2502.10816*, 2025. 1
- [50] Wenxin Xu, Hexin Jiang, et al. Leveraging knowledge of modality experts for incomplete multimodal learning. In *ACM Multimedia 2024*, 2024. 1, 2, 6, 7, 3
- [51] Ziqi Yuan, Yihe Liu, Hua Xu, and Kai Gao. Noise imitation based adversarial training for robust multimodal sentiment analysis. *IEEE Transactions on Multimedia*, 26:529–539, 2023. 2
- [52] AmirAli Bagher Zadeh, Paul Pu Liang, Soujanya Poria, Erik Cambria, and Louis-Philippe Morency. Multimodal language analysis in the wild: Cmu-mosei dataset and interpretable dynamic fusion graph. In *Proceedings of the 56th Annual Meeting of the Association for Computational Linguistics (Volume 1: Long Papers)*, pages 2236–2246, 2018. 6, 2
- [53] Kaipeng Zhang, Zhanpeng Zhang, Zhifeng Li, and Yu Qiao. Joint face detection and alignment using multitask cascaded convolutional networks. *IEEE signal processing letters*, 23(10):1499–1503, 2016. 3
- [54] Qingyang Zhang, Yake Wei, Zongbo Han, Huazhu Fu, Xi Peng, Cheng Deng, Qinghua Hu, Cai Xu, Jie Wen, Di Hu, et al. Multimodal fusion on low-quality data: A comprehensive survey. *arXiv preprint arXiv:2404.18947*, 2024. 1, 2, 5

- [55] Binyu Zhao, Wei Zhang, and Zhaonian Zou. Mce: Towards a general framework for handling missing modalities under imbalanced missing rates. *Pattern Recognition*, page 112591, 2025. [2](#), [6](#), [3](#)
- [56] Jinming Zhao, Ruichen Li, and Qin Jin. Missing modality imagination network for emotion recognition with uncertain missing modalities. In *Proceedings of the 59th Annual Meeting of the Association for Computational Linguistics*, pages 2608–2618, 2021. [1](#), [2](#), [6](#), [7](#), [3](#)
- [57] Zengqun Zhao, Qingshan Liu, and Shanmin Wang. Learning deep global multi-scale and local attention features for facial expression recognition in the wild. *IEEE Transactions on Image Processing*, 30:6544–6556, 2021. [3](#)

# BALM: A Model-Agnostic Framework for Balanced Multimodal Learning under Imbalanced Missing Rates

## Supplementary Material

### A. Training procedure of BALM

The overall training procedure of BALM, including both the feature calibration and gradient rebalancing stages, is summarized in Algorithm 1.

---

**Algorithm 1** Training procedure of the proposed plug-in framework BALM

---

**Require:** Multimodal dataset  $\mathbb{D}$ ; model  $(\phi^m, \mathcal{F}, \mathbf{F}_{pred})$ ; missing rates  $\mathbf{r} = (r_a, r_v, r_l)$ ; total epochs  $E$ ; hyper-parameters  $\tau, \rho, \alpha$ .

- 1: Initialize modulation loss  $\mathcal{L}_{mod} \leftarrow 0$  and iteration  $t \leftarrow 0$
- 2: Generate missing mask  $e \sim \mathcal{M}(x; \mathbf{r})$
- 3: Generate incomplete dataset  $\tilde{\mathbb{D}} \leftarrow \{(\tilde{x}_i, y_i)\}$
- 4: **for**  $epoch = 1$  **to**  $E$  **do**
- 5:     **for** each  $(\tilde{x}_i, y_i) \in \tilde{\mathbb{D}}$  **do**
- 6:         **Calibrate** unimodal features:  $\hat{x}_i^m \leftarrow \text{FCM}(\tilde{x}_i)$
- 7:         **Encode** modalities:  $z_i^m \leftarrow \text{Eq. 11}$
- 8:         **Fuse** embeddings:  $h_i \leftarrow \text{Eq. 12}$
- 9:         **Compute** multimodal prediction:  $\hat{y}_i \leftarrow \text{Eq. 13}$
- 10:         **Compute** task loss:  $\mathcal{L}_{task} \leftarrow \text{Eq. 14}$
- 11:         **Aggregate** total loss:  $\mathcal{L} \leftarrow \mathcal{L}_{task} + \tau \mathcal{L}_{mod}$
- 12:         **Update** parameters:  $\theta \leftarrow \theta - \alpha \nabla_{\theta} \mathcal{L}$
- 13:         **Compute** unimodal predictions:  $\hat{y}_i^m \leftarrow \text{Eq. 17}$
- 14:         **Compute** unimodal loss:  $\mathcal{L}_{task}^m \leftarrow \text{Eq. 18}$
- 15:         **Estimate** coefficients:  $\mu^m \leftarrow \text{Eq. 21}$
- 16:         **Modulate** encoder gradients:  $\theta^{\phi^m} \leftarrow \text{Eq. 22}$
- 17:         **Update** spatial modulation loss:  $\mathcal{L}_{mod} \leftarrow \text{Eq. 26}$
- 18:          $t \leftarrow t + 1$
- 19:     **end for**
- 20: **end for**

---

### B. Theoretical Analysis

#### B.1. Gradient Imbalance under IMR

This section provides a formal justification for Eq. 6 in the main paper, showing how the imbalance in gradient magnitudes arises under the Imbalanced Missing Rate (IMR) condition.

**Assumption 1 (Independent Missingness).** Each modality  $m$  is independently missing according to a Bernoulli variable  $e_i^m \in \{0, 1\}$  with  $P(e_i^m = 1) = (1 - r_m)$  and  $P(e_i^m = 0) = r_m$ , where  $r_m \in [0, 1)$  denotes the missing probability of modality  $m$ . The missingness indicators  $\{e_i^m\}$  are assumed independent of the target label  $Y$  (i.e., Missing Completely At Random-MCAR).

**Lemma 1 (Expected Gradient Scaling under IMR).** Under above Assumption, for a differentiable per-sample loss  $\ell_m = \ell(f_m(X_m), Y)$  with finite variance, the expected gradient of modality  $m$  with respect to its parameters  $\theta_m$  satisfies:

$$\mathbb{E}[\nabla_{\theta_m} \mathcal{L}_{\text{IMR}}] = (1 - r_m) \mathbb{E}[\nabla_{\theta_m} \ell(f_m(X_m), Y)]. \quad (28)$$

*Proof.* Let  $\mathcal{L}_{\text{IMR}}$  denote the expected loss under the IMR distribution:

$$\mathcal{L}_{\text{IMR}} = \mathbb{E}_{X, Y, e} \left[ \sum_{m=1}^M e^m \ell(f_m(X_m; \theta_m), Y) \right], \quad (29)$$

where  $f_m(\cdot; \theta_m)$  represents the modality-specific encoder or prediction branch parameterized by  $\theta_m$ , and  $e^m$  indicates its availability. Taking the gradient with respect to  $\theta_m$  yields:

$$\nabla_{\theta_m} \mathcal{L}_{\text{IMR}} = \mathbb{E}_{X, Y, e} [e^m \nabla_{\theta_m} \ell(f_m(X_m; \theta_m), Y)]. \quad (30)$$

By the linearity of expectation, we can separate the stochastic variable  $e^m$ :

$$\mathbb{E}[\nabla_{\theta_m} \mathcal{L}_{\text{IMR}}] = \mathbb{E}_e [e^m] \mathbb{E}_{X, Y} [\nabla_{\theta_m} \ell(f_m(X_m; \theta_m), Y)]. \quad (31)$$

Since  $e^m \sim \text{Bernoulli}(1 - r_m)$ , we have  $\mathbb{E}[e^m] = 1 - r_m$ . Substituting this into Eq. 31 gives:

$$\mathbb{E}[\nabla_{\theta_m} \mathcal{L}_{\text{IMR}}] = (1 - r_m) \mathbb{E}[\nabla_{\theta_m} \ell(f_m(X_m; \theta_m), Y)]. \quad (32)$$

Eq. 32 shows that, in expectation, the gradient propagated to the parameters  $\theta_m$  of each modality-specific encoder is linearly scaled by its availability ratio  $(1 - r_m)$ .

**Corollary 1 (Gradient Imbalance Effect).** Taking the  $L_2$  norm of Eq. 32 yields

$$\mathbb{E}[\|\nabla_{\theta_m} \mathcal{L}_{\text{IMR}}\|] = (1 - r_m) \mathbb{E}[\|\nabla_{\theta_m} \ell(f_m(X_m; \theta_m), Y)\|]. \quad (33)$$

Therefore, modalities with higher missing rates ( $r_m$  large) receive proportionally weaker gradient updates on their encoder parameters, causing slower convergence and optimization dominance by low-missing-rate modalities.

The above analysis reveals that, under IMR, each modality receives a gradient update scaled by its availability ratio  $(1 - r_m)$ . This induces biased optimization dynamics where dominant modalities converge faster while rare ones lag behind. To counteract this imbalance, the Gradient

Rebalancing Module (GRM) introduced later (Eq. 21 and Eq. 22) adaptively rescales the gradient flow through modulation coefficients  $\mu_m$  that act as an inverse correction to the implicit scaling factor  $(1 - r_m)$ . In essence, GRM restores equilibrium among modalities by dynamically adjusting both the magnitude and the direction of their gradients, thereby stabilizing multimodal optimization under heterogeneous missing conditions.

## B.2. Gradient Rebalancing Rationale

**Proposition 1.** Building on **Lemma 1**, which shows that the expected gradient magnitude of each modality is scaled by its availability ratio  $(1 - r_m)$ , we explain the rationale behind the proposed Gradient Rebalancing Module (GRM). **Rationale.** GRM compensates for the imbalance in gradient magnitudes through adaptive modulation of each modality’s update:

$$\begin{aligned} \mu^m &= \rho \frac{\sum_{m' \in \{a,v,l\}, m' \neq m} \Delta_{\text{KL}}^{m'}}{\sum_{m' \in \{a,v,l\}} \Delta_{\text{KL}}^{m'}}, \\ \theta_{(t+1)}^{\phi^m} &= \theta_{(t)}^{\phi^m} - \alpha \mu^m \frac{\partial \mathcal{L}_{\text{task}}}{\partial \theta_{(t)}^{\phi^m}}. \end{aligned} \quad (34)$$

Here,  $\Delta_{\text{KL}}^m$  quantifies the learning discrepancy of modality  $m$  between its unimodal and fused distributions, and  $\rho$  is a hyperparameter controlling the modulation intensity. A smaller  $\mu^m$  indicates that modality  $m$  is learning faster (*i.e.*, larger  $\Delta_{\text{KL}}^m$ ) and thus its gradient update is attenuated, whereas slower modalities are amplified. This mechanism counteracts the imbalance identified in Lemma 1 and encourages all modality-specific gradients to approach an equilibrium:

$$\|\mu^m \nabla_{\theta^{\phi^m}} \mathcal{L}_{\text{task}}\| \approx \|\mu^{m'} \nabla_{\theta^{\phi^{m'}}} \mathcal{L}_{\text{task}}\|, \quad \forall m, m'. \quad (35)$$

Here,  $\nabla_{\theta^{\phi^m}} \mathcal{L}_{\text{task}}$  denotes the gradient of the task loss with respect to the parameters of the  $m$ -th encoder, and  $\|\cdot\|$  denotes the Euclidean norm measuring its magnitude.

Such modulation is consistent with previous analyses [8, 29] showing that gradient reweighting based on learning discrepancy stabilizes multimodal training. GRM extends this idea to imbalanced missing-rate conditions, using KL-divergence as a continuous signal of learning disparity rather than a fixed prior ratio  $(1 - r_m)$ .

## C. Benchmark Datasets

### C.1. Dataset Description

To evaluate the effectiveness of BALM, we conduct experiments on two widely used multimodal emotion and sentiment benchmarks: IEMOCAP [3] and CMU-MOSEI [52]. Their key statistics are summarized in Table 5.

Table 5. Statistical overview of the IEMOCAP and CMU-MOSEI datasets.

Dataset	Dialogues			Utterances		
	train	valid	test	train	valid	test
<b>IEMOCAP</b>	120	31		5810	1623	
<b>CMU-MOSEI</b>	2249	300	676	16326	1871	4659

**IEMOCAP** contains dyadic interactions between actors performing both scripted and improvised dialogues designed to elicit diverse emotions. The corpus comprises five sessions, each segmented into multiple utterances annotated with categorical emotion labels. Following the label processing in [25], we adopt the common six-class setting. Since the original dataset only provides training and test splits, we further divide the training set into training and validation subsets using a ratio of  $r$  (default 0.1).

**CMU-MOSEI** consists of 22,856 video-based utterances from over 1,000 YouTube speakers, each annotated with a sentiment score in the range  $[-3, 3]$ . Following [19], this dataset is trained as regression task, and evaluated as negative/positive classification task. Positive and negative classes are assigned for  $< 0$  and  $> 0$  scores, respectively. The official partitioning protocol is adopted to ensure consistency with previous studies.

Similar to prior studies [11, 13, 27], we use Accuracy (Acc) and Weighted F1 Score (W-F1) as our main evaluation metrics.

### C.2. Multimodal Feature Extraction

For each utterance, multimodal features are extracted from acoustic, lexical, and visual modalities. The details of the extraction process for the two datasets are described as follows.

For the **IEMOCAP** dataset, we follow the feature extraction procedures outlined in [25] to obtain feature vectors for each modality. Specifically, we employ the RoBERTa-Large [23] model to extract 1024-dimensional textual features. RoBERTa is fine-tuned for emotion recognition on conversation transcripts, and the embeddings of the [CLS] tokens from the last layer are used as textual representations. Acoustic features are extracted using openSMILE [6] and then reduced to 1,582 dimensions via a fully connected layer, while visual features are obtained from a pre-trained DenseNet [15], resulting in 342-dimensional representations for each utterance.

Similarly, we adopt the feature extraction methods described in [19] for **CMU-MOSEI**. Pre-trained wav2vec<sup>4</sup> [32] is leveraged to extract 512-dimensional acoustic features for each utterance. For the textual modality, the pre-

<sup>4</sup><https://github.com/pytorch/fairseq/tree/main/examples/wav2vec>

trained DeBERTa-Large model<sup>5</sup> [9] is exploited to encode word sequences into 1024-dimensional representations. Visual features are obtained through a two-step process: faces are first detected and aligned using the MTCNN [53] face detection algorithm, and the aligned frames are subsequently processed with MA-Net<sup>6</sup> [57] to produce frame-level features. Finally, we aggregate these frame-level facial features into 1024-dimensional utterance-level representations using average pooling.

## D. Baseline Models

To evaluate the performance of BALM, we compare it with state-of-the-art methods for incomplete or imbalanced multimodal learning, as well as typical MER backbones.

### D.1. Incomplete or Imbalanced Multimodal Models

The following baselines focus on addressing the challenges of missing modalities and uneven multimodal contribution.

**MMIN** [56] learns robust joint representations by imagining the features of absent modalities from the available ones via cycle-consistent autoencoders, thereby handling uncertain missing conditions effectively.

**SDR-GNN** [7] integrates spectral analysis into a hyper-graph framework to impute missing data and explicitly retains high-frequency signals typically lost in conventional GNNs.

**Mi-CGA** [28] utilizes a reconstruction module to approximate missing inputs and leverages cross-modal graph attention to capture comprehensive inter-modal dependencies.

**MoMKE** [50] adopts a dual-phase learning scheme in which a learnable router dynamically fuses outputs from pretrained unimodal encoders to derive a more comprehensive representation for incomplete data.

**GCNet** [19] captures speaker and temporal dependencies via graph neural networks to handle incomplete conversations and employs a dual-task framework to simultaneously predict target labels and restore missing features.

**Ada2I** [27] rectifies learning imbalances by dynamically re-weighting feature and modality contributions under the supervision of a learning discrepancy metric.

**RedCore** [34] employs variational encoders to construct robust cross-modal representations and dynamically regulates auxiliary supervision based on reconstruction difficulty.

**MCE** [55] optimizes training dynamics via game-theoretic evaluations and promotes semantic robustness through subset prediction to facilitate balanced feature capability despite imbalanced missing rates.

Table 6. Hyper-parameters Setting

Parameters	IEMOCAP	CMU-MOSEI
Audio dim $d_a$	1582	512
Lexical dim $d_l$	1024	1024
Visual dim $d_v$	342	1024
$d_{\text{global}}$	737	640
$\rho$	(1.1,1.6]	
$\tau$	(0.2,0.8]	
batch size	16	32
epoch	80	25

### D.2. MER Backbones

To assess overall effectiveness, we further compare against mainstream backbones renowned for their multimodal context modeling and fusion mechanisms.

**MMGCN** [13] leverages a deep spectral graph network to fuse multimodal features. The framework defines utterances as interconnected nodes and captures long-range dependencies along with speaker context for emotion classification.

**MMDFN** [11] employs a gated graph architecture to selectively regulate cross-modal information flow. By dynamically filtering feature propagation across layers, it mitigates the accumulation of redundant data while strengthening inter-modal synergy.

## E. Implementation Details

We conduct experiments under varying missing configurations to evaluate the performance of different baselines on multimodal emotion recognition datasets. For each dataset  $\mathbb{D}$  and missing setting  $\mathbf{r} = (r_A, r_L, r_V)$ , we generate modality-missing masks  $e$  for the train/validation/test sets independently using the masking operator  $\mathcal{M}(\cdot, \mathbf{r})$ . Masking is applied prior to any processing or training, ensuring that complete data remain hidden from all models during both training and inference, while the missing masks remain fixed. The best model selected on the incomplete validation set is then evaluated on the incomplete test set.

For all baselines, we adopt their official implementations and model-specific hyperparameter settings (including learning rates) provided in their documentation. For **GCNet**, **SDR-GNN**, and **Mi-CGA**, specifically, we employ variants that omit reconstruction losses to ensure no baseline has access to any complete data.

For integrating **BALM** to **GCNet**, **MMGCN**, and **MMDFN**, FCM is added as a additional module to their architect while GCM is used as a separated module monitoring the training phase, the unimodal prediction heads is trained in parallel with the backbone using the same optimizer and learning rate, main architect and hyper-parameters of the backbone remain unchanged. Since **CMU-MOSEI** is

<sup>5</sup><https://huggingface.co/microsoft/deberta-large>

<sup>6</sup><https://github.com/zengqunzhao/MA-Net>

Table 7. Weighted-F1 sensitivity to hyperparameters under two contrastive missing-rate configurations of audio, language and visual.

Config A (0.5, 0.3, 0.7)		$\rho$				Config B (0.5, 0.7, 0.3)		$\rho$					
		1.0	1.2	1.4	1.6			1.8	1.0	1.2	1.4	1.6	1.8
$\tau$	0.1	64.38	64.92	63.71	63.90	65.93	$\tau$	0.1	59.49	61.37	<b>62.41</b>	59.39	61.26
	0.4	65.50	64.71	65.53	63.80	64.31		0.4	59.98	60.62	61.80	60.22	60.45
	0.7	64.88	64.14	63.59	64.14	63.57		0.7	60.21	59.05	60.86	61.34	59.11
	1.0	65.10	63.71	64.26	<b>66.30</b>	65.67		1.0	60.35	60.58	60.73	59.48	59.87
	1.3	63.64	64.50	64.03	64.16	64.37		1.3	61.34	60.21	59.02	58.39	59.09

treated as a regression task, we omit the softmax function ( $\delta(\cdot)$  in Eq. 13, Eq. 17) and use sigmoid function to map predicted scalars to probabilities of negative/positive class for Distribution-driven Modulation in GRM.

All experiments are implemented in PyTorch<sup>7</sup>, and tracked with Comet.ml<sup>8</sup>. Additional training configurations and hyper-parameters of BALM are summarized in Table 6.

**Code Availability and Reproducibility.** We release our full implementation and configurations at: [https://github.com/np4s/BALM\\_CVPR2026.git](https://github.com/np4s/BALM_CVPR2026.git). The repository includes source code, configuration files, and brief guidelines with scripts to run experiments or adapt the framework to other datasets.

**Masking Operator.** Given a dataset of  $N$  samples with  $M$  modalities and a missing-ratio vector  $\mathbf{r} = [r_1, \dots, r_M]$ , our masking operator  $\mathcal{M}(\cdot; \mathbf{r})$  generates missing masks based on the hypothetical ratios of missing patterns. For a missing pattern  $\hat{e} = [\hat{e}^1, \dots, \hat{e}^M]$  among the  $2^M$  possible patterns, its ratio is computed as:

$$\hat{r} = \prod_{m=1}^M \hat{e}^m (1 - r_m) \times (1 - \hat{e}^m) r_m. \quad (36)$$

Thus,  $n = \lfloor N \hat{r} \rfloor$  samples are randomly assigned to the missing pattern  $\hat{e}$ , generating  $n$  missing-mask vectors with  $e_i = \hat{e}$ . Since each sample must retain at least one modality, the  $N \prod_{m=1}^M r_m$  masks corresponding to the pattern where all modalities are missing are redistributed uniformly among the  $M$  patterns where exactly  $M - 1$  modalities are missing. Consequently, the error  $\varepsilon_m$  of  $\mathcal{M}(\cdot; \mathbf{r})$ , defined as the discrepancy between the intended missing ratio  $r_m$  and the realized missing ratio  $\frac{1}{N} \sum_{i=1}^N (1 - e_i^m)$  for modality  $m$ , satisfies  $\varepsilon_m \leq \frac{1}{M} \prod_{m'=1}^M r_{m'}$ .

## F. Additional Experiment Results

### F.1. Hyperparameter Sensitivity under Contrasting Missing Rates (Detailed Results)

Table 7 provides the complete numerical results of MMGCN+BALM on IEMOCAP for the two contrasting IMR

<sup>7</sup><https://pytorch.org/>

<sup>8</sup><https://comet.ml>

configurations.

Specifically, under *Config-A* (0.5, 0.3, 0.7), w-F1 remains stable across the  $(\tau, \rho)$  grid, mostly lying within 63–64%, with limited sensitivity to either hyperparameter. The best score 66.30% occurs at  $(\tau=1.0, \rho=1.6)$ , while all other settings fluctuate within a narrow range of about 2%.

In contrast, *Config-B* (0.5, 0.7, 0.3) shows noticeably larger spread, ranging from 58.39% to 62.41%. Performance improves around small  $\tau$  with moderate  $\rho$  (best at  $(\tau=0.1, \rho=1.4)=62.41\%$ ), whereas higher  $\rho$  consistently leads to degradation across all  $\tau$ . This pattern indicates stronger  $\tau$ - $\rho$  interaction when the lexical modality has the highest missing rate.

### F.2. Average performance on different modality combinations (Detailed Results)

Table 8 and Table 9 report the complete results for Accuracy (Acc) and weighted-F1 (w-F1), respectively, across all modality combinations—*unimodal* (A, V, L), *bimodal* (AV, AL, LV), and *trimodal* (ALV)—under different missing-rate settings on IEMOCAP. For each combination, unspecified modalities are ablated from training and evaluating. We compare GCNet and MMGCN with their variants enhanced by BALM. Across all unimodal, bimodal, and trimodal configurations, the BALM-enhanced models consistently achieve higher Acc and W-F1, demonstrating improved robustness under varying missing-modality conditions. The averaged performance across all configurations is presented in Fig. 6 of the main paper.

Table 10 reports the full MMGCN results across all modality combinations before and after integrating the FCM module. In this experiment, MMGCN and MMGCN+BALM are trained under the specified condition and tested on the complete test-set of modality combinations. The averaged performance is summarized in Table 3 of the main paper. Overall, FCM provides consistent improvements across settings, highlighting the effectiveness of BALM in addressing the inconsistent representations arising from IMR.

### F.3. BALM under SMR settings (Numerical Results)

Table 11 and Table 12 report the detail results from Fig. 4 in the main paper. By addressing challenges of missing modalities with BALM, MMGCN+BALM and MMDFN+BALM are

Table 8. Performance across unimodal, bimodal, and trimodal configurations under varying missing rates (Accuracy)

MR Setting	Model	A	V	L	AV	AL	LV	ALV
(0.5, 0.5, 0.7)	GCNet	46.33	37.28	57.42	48.18	59.09	54.16	58.47
	GCNet <sub>+BALM</sub>	46.95	31.44	59.09	50.89	59.64	54.41	59.33
	MMGCN <sub>+BALM</sub>	51.45	31.98	60.63	46.77	61.18	62.60	60.44
(0.5, 0.7, 0.5)	GCNet	49.04	31.85	56.99	48.49	56.69	53.73	57.86
	GCNet <sub>+BALM</sub>	47.13	27.60	54.59	46.21	58.10	55.76	55.82
	MMGCN <sub>+BALM</sub>	51.02	29.94	59.89	51.26	62.23	52.50	61.49
(0.7, 0.5, 0.5)	GCNet	44.18	30.19	56.44	38.32	56.93	56.81	58.23
	GCNet <sub>+BALM</sub>	48.37	30.75	56.90	47.57	60.01	58.60	57.86
	MMGCN <sub>+BALM</sub>	48.92	29.94	62.97	46.03	62.54	60.07	62.85
(0.3, 0.5, 0.7)	GCNet	47.87	32.72	53.54	48.55	60.20	55.51	59.46
	GCNet <sub>+BALM</sub>	51.57	32.10	54.53	53.05	60.38	54.53	61.12
	MMGCN <sub>+BALM</sub>	52.93	28.34	60.57	52.43	62.78	60.38	62.78
(0.5, 0.3, 0.7)	GCNet	45.41	32.35	59.64	45.96	59.64	57.92	58.60
	GCNet <sub>+BALM</sub>	51.26	35.00	59.64	51.76	61.80	60.20	60.69
	MMGCN <sub>+BALM</sub>	50.89	28.34	63.71	50.40	64.08	61.31	64.39
(0.7, 0.5, 0.3)	GCNet	46.89	35.49	54.47	48.86	56.01	54.78	58.41
	GCNet <sub>+BALM</sub>	44.55	35.43	55.51	52.00	54.10	55.88	59.33
	MMGCN <sub>+BALM</sub>	45.96	28.90	61.61	46.95	61.86	59.09	61.74
Average	GCNet	46.62	<b>33.31</b>	56.42	46.39	58.09	55.49	58.51
	GCNet <sub>+BALM</sub>	48.31	32.05	56.71	<b>50.25</b>	59.01	56.56	59.02
	MMGCN <sub>+BALM</sub>	<b>50.20</b>	29.57	<b>61.56</b>	48.97	<b>62.45</b>	<b>59.33</b>	<b>62.28</b>

Table 9. Performance across unimodal, bimodal, and trimodal configurations under varying missing rates (w-F1)

MR Setting	Model	A	V	L	AV	AL	LV	ALV
(0.5, 0.5, 0.7)	GCNet	45.91	34.50	57.76	48.44	59.06	54.02	58.52
	GCNet <sub>+BALM</sub>	46.56	27.57	59.47	50.56	59.77	53.93	59.51
	MMGCN <sub>+BALM</sub>	50.66	25.81	61.05	48.66	60.44	62.12	60.39
(0.5, 0.7, 0.5)	GCNet	44.14	29.65	56.58	49.40	56.71	53.81	58.15
	GCNet <sub>+BALM</sub>	48.36	26.36	54.82	46.89	58.36	56.05	58.75
	MMGCN <sub>+BALM</sub>	50.07	28.88	59.50	51.01	61.85	51.77	61.37
(0.7, 0.5, 0.5)	GCNet	42.68	25.13	56.54	35.41	57.30	57.26	58.35
	GCNet <sub>+BALM</sub>	45.31	26.62	54.77	46.54	59.99	58.63	58.01
	MMGCN <sub>+BALM</sub>	48.85	28.88	62.18	46.00	62.08	60.29	62.78
(0.3, 0.5, 0.7)	GCNet	43.77	32.29	52.87	48.67	60.68	54.84	59.40
	GCNet <sub>+BALM</sub>	50.54	28.40	54.75	51.26	60.57	54.52	61.40
	MMGCN <sub>+BALM</sub>	52.51	26.86	60.95	51.91	62.73	60.61	62.17
(0.5, 0.3, 0.7)	GCNet	43.47	32.25	59.85	44.77	60.09	57.73	58.88
	GCNet <sub>+BALM</sub>	49.61	34.11	59.75	50.92	62.21	60.43	60.78
	MMGCN <sub>+BALM</sub>	50.87	26.86	63.64	50.33	63.28	61.33	63.73
(0.7, 0.5, 0.3)	GCNet	46.08	33.43	54.02	49.48	56.14	54.54	58.61
	GCNet <sub>+BALM</sub>	42.91	32.98	55.51	51.46	54.09	56.45	58.98
	MMGCN <sub>+BALM</sub>	45.19	25.48	61.54	50.63	61.15	59.21	61.92
Average	GCNet	44.34	<b>31.21</b>	56.27	46.03	58.33	55.37	58.65
	GCNet <sub>+BALM</sub>	47.22	29.34	56.51	49.61	59.17	56.67	59.57
	MMGCN <sub>+BALM</sub>	<b>49.69</b>	27.13	<b>61.48</b>	<b>49.76</b>	<b>61.92</b>	<b>59.22</b>	<b>62.06</b>

able to achieve a more robust performance as the shared missing rate increases. Notably, for IEMOCAP, other methods addressing missing modalities can suffer up to over 3% performance reduction, e.g. SDR-GNN and GCNet when SMR increase from 0.5 to 0.6, Mi-CGA when SMR increase from 0.6 to 0.7; while both MMGCN<sub>+BALM</sub> and MMDFN<sub>+BALM</sub> only see a 1% – 2% drop across missing rates. Although more subtle, such trend in the performance’s consistency can also be seen for CMU-MOSEI.

#### F.4. Gradient Rebalancing Module Analysis

To further investigate the two sub-modules of Gradient Rebalancing Module (GRM), we introduce two variants: **BALM-D** consisting FCM and *distribution modulation* only, and its counterpart **BALM-S** consisting FCM and *spatial modulation* only.

Fig. 8 shows the learning progress of the modalities during training under IMR setting  $(r_A, r_L, r_V) = (0.5, 0.7, 0.3)$ , while Table 13 displays quantitative performance of the two variants. The more robust and over-

Table 10. Performance of MMGCN on different modality combinations after training under IMR setting  $(r_A, r_L, r_V) = (0.5, 0.7, 0.3)$ , before and after plugged with FCM module.

Modality	IEMOCAP				CMU-MOSEI			
	MMGCN		+FCM		MMGCN		+FCM	
	Acc	w-F1	Acc	w-F1	Acc	w-F1	Acc	w-F1
A	31.05	25.97	39.99	34.75	62.85	48.51	62.85	48.51
L	61.92	61.01	62.48	61.56	83.46	83.68	85.75	85.76
V	19.78	11.67	20.70	12.07	62.91	48.66	62.85	50.06
AL	64.45	63.11	63.77	62.15	83.57	83.78	85.72	85.71
AV	32.29	26.92	42.88	38.07	62.91	48.64	62.85	48.86
LV	61.98	61.03	62.91	61.92	85.39	85.40	85.91	85.87
ALV	65.19	63.94	64.20	62.80	85.55	85.55	85.88	85.83
<b>Avg.</b>	<b>48.09</b>	<b>44.81</b>	<b>50.99</b>	<b>47.62</b>	<b>75.23</b>	<b>69.17</b>	<b>75.97</b>	<b>70.09</b>

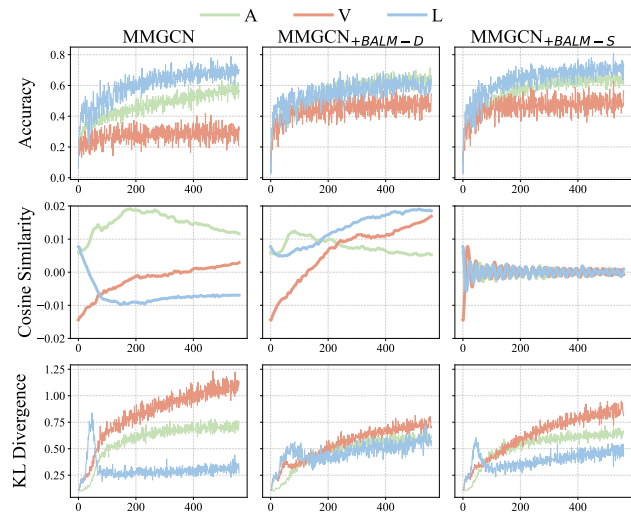


Figure 8. Modality discrepancies on IEMOCAP with different variants of BALM.

all better performance of MMGCN+BALM (from Table 1, 2 in main paper) when compared to MMGCN+BALM-D and MMGCN+BALM-S further highlight the complementary nature of *distribution-* and *spatial-driven* Modulation. Fig. 8 suggests that these two-sided modulations act as each other’s regulator, keeping the backbone from being over-balanced toward either perspective (e.g., the cosine similarity of MMGCN+BALM-S), thus, giving a more general model.

## F.5. Distribution-driven Modulation Analysis

We introduce the BALM-M variant, in which the KL divergence (i.e.,  $\text{KL}(\cdot)$  in Eq. 19) is replaced with an Mean Squared Error (MSE) loss, while all other computations in GRM remain unchanged. Detailed results for GCNet+BALM-M, MMGCN+BALM-M, and MMDFN+BALM-M, along with their performance gaps relative to the corresponding baseline enhanced by BALM, are reported in Ta-

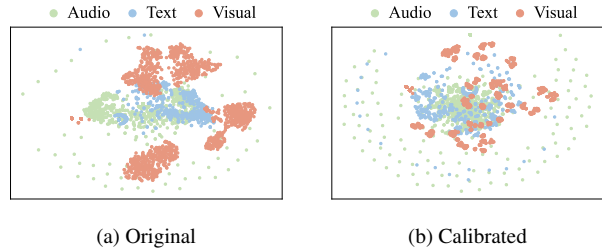


Figure 8. Original input of MMGCN (i.e.,  $\hat{x}$ ) and calibrated input of MMGCN+BALM (i.e.,  $\hat{x}$ ), under IMR setting  $(r_A, r_L, r_V) = (0.5, 0.7, 0.3)$  on IEMOCAP.

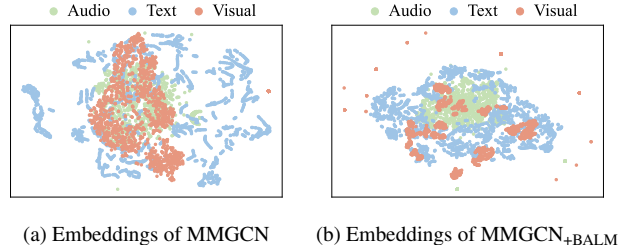


Figure 9. The embeddings (i.e.,  $z$  in Eq. 11) corresponding to the inputs from Fig. 8.

ble 14 and Table 15.

The improvements observed in MMDFN+BALM-M over MMDFN+BALM under most settings on IEMOCAP, up to 1.67% under  $(0.3, 0.5, 0.7)$ , suggest that MSE can also serve as an effective measure of the distribution gap between multimodal and unimodal predictions for certain backbones. Nonetheless, KL divergence consistently yields better performance across different backbones and across both datasets, likely due to its softer characterization of distribution differences, verifies its advantage as a more suitable choice for distribution quantification as we aim to generalize BALM across diverse models.

## F.6. Multimodal Representation

Fig. 8, 9, 10 visualize the features comparison at different stages between MMGCN and MMGCN+BALM using t-SNE. As Fig. 8 depicts, after being calibrated with FCM, the outliers of audio and lexical modalities become more visible, which is a better reflection of the dataset’s properties in this specific scenario where these two modalities suffer loss at high rates, while visual features are also preprocessed into more defined clusters. Consequently, the embeddings in Fig. 9 also show a better learning of modal-specific encoders, resulting in multimodal fused feature with more distinct border between *hap-exc* (happy - excited) and *ang-fru* (angry - frustrated) clusters in Fig. 10.

Table 11. Average performance of five runs under different SMR settings on IEMOCAP.

SMR	Mi-CGA		SDR-GNN		GCNet		MMGCN <sub>+BALM</sub>		MMDFN <sub>+BALM</sub>	
	Acc	w-F1	Acc	w-F1	Acc	w-F1	Acc	w-F1	Acc	w-F1
0.0	64.45 $\pm$ 0.76	64.49 $\pm$ 0.94	64.86 $\pm$ 0.78	64.65 $\pm$ 0.83	64.90 $\pm$ 0.59	65.01 $\pm$ 0.68	65.63 $\pm$ 1.92	65.49 $\pm$ 1.90	70.02 $\pm$ 0.95	69.89 $\pm$ 0.81
0.1	63.43 $\pm$ 1.27	63.42 $\pm$ 1.24	63.43 $\pm$ 1.07	63.35 $\pm$ 0.99	64.10 $\pm$ 0.73	63.99 $\pm$ 0.63	64.28 $\pm$ 0.71	64.05 $\pm$ 0.74	68.90 $\pm$ 0.99	68.78 $\pm$ 1.06
0.2	63.71 $\pm$ 1.68	63.76 $\pm$ 1.68	62.28 $\pm$ 1.48	62.00 $\pm$ 1.41	63.18 $\pm$ 1.57	62.83 $\pm$ 1.67	63.73 $\pm$ 1.84	63.54 $\pm$ 1.89	68.56 $\pm$ 0.73	68.45 $\pm$ 0.72
0.3	60.46 $\pm$ 1.26	59.93 $\pm$ 1.46	60.54 $\pm$ 3.23	59.92 $\pm$ 2.92	62.50 $\pm$ 0.61	62.14 $\pm$ 0.80	62.76 $\pm$ 1.16	62.67 $\pm$ 1.21	67.43 $\pm$ 1.38	67.44 $\pm$ 1.37
0.4	59.99 $\pm$ 1.96	60.18 $\pm$ 2.02	59.16 $\pm$ 1.25	58.85 $\pm$ 1.16	60.31 $\pm$ 1.01	60.01 $\pm$ 1.38	62.12 $\pm$ 0.97	61.90 $\pm$ 0.94	66.21 $\pm$ 0.98	66.15 $\pm$ 0.95
0.5	58.07 $\pm$ 1.49	58.09 $\pm$ 1.64	58.79 $\pm$ 2.18	58.20 $\pm$ 1.71	58.68 $\pm$ 0.85	58.54 $\pm$ 0.80	61.77 $\pm$ 1.53	61.82 $\pm$ 1.72	64.93 $\pm$ 1.47	64.78 $\pm$ 1.48
0.6	58.43 $\pm$ 1.09	58.42 $\pm$ 1.26	55.71 $\pm$ 2.32	55.27 $\pm$ 2.15	55.00 $\pm$ 2.37	54.83 $\pm$ 2.47	60.75 $\pm$ 1.93	60.71 $\pm$ 1.94	63.64 $\pm$ 2.33	63.27 $\pm$ 2.29
0.7	55.79 $\pm$ 0.85	55.40 $\pm$ 1.67	54.41 $\pm$ 2.47	53.65 $\pm$ 2.46	53.91 $\pm$ 0.83	53.52 $\pm$ 1.21	59.68 $\pm$ 2.09	59.59 $\pm$ 2.20	61.63 $\pm$ 2.36	61.80 $\pm$ 2.15

Table 12. Average performance of five runs under different SMR settings on CMU-MOSEI.

SMR	Mi-CGA		SDR-GNN		GCNet		MMGCN <sub>+BALM</sub>		MMDFN <sub>+BALM</sub>	
	Acc	w-F1	Acc	w-F1	Acc	w-F1	Acc	w-F1	Acc	w-F1
0.0	86.23 $\pm$ 0.44	86.21 $\pm$ 0.35	86.60 $\pm$ 0.56	86.58 $\pm$ 0.51	87.00 $\pm$ 0.32	86.94 $\pm$ 0.39	87.33 $\pm$ 0.16	87.29 $\pm$ 0.19	86.98 $\pm$ 0.38	86.96 $\pm$ 0.36
0.1	85.06 $\pm$ 0.43	85.04 $\pm$ 0.50	85.82 $\pm$ 0.30	85.80 $\pm$ 0.31	85.92 $\pm$ 0.29	85.87 $\pm$ 0.23	85.81 $\pm$ 0.22	85.73 $\pm$ 0.16	86.13 $\pm$ 0.53	86.06 $\pm$ 0.50
0.2	83.60 $\pm$ 0.68	83.47 $\pm$ 0.56	84.85 $\pm$ 0.36	84.77 $\pm$ 0.34	84.57 $\pm$ 0.83	84.56 $\pm$ 0.71	85.55 $\pm$ 0.19	85.45 $\pm$ 0.18	84.78 $\pm$ 0.36	84.65 $\pm$ 0.34
0.3	82.26 $\pm$ 0.50	82.23 $\pm$ 0.47	83.34 $\pm$ 0.39	83.18 $\pm$ 0.26	83.83 $\pm$ 0.30	83.73 $\pm$ 0.29	83.90 $\pm$ 0.22	83.67 $\pm$ 0.34	83.87 $\pm$ 0.13	83.80 $\pm$ 0.18
0.4	81.33 $\pm$ 0.38	81.19 $\pm$ 0.42	82.35 $\pm$ 0.56	81.99 $\pm$ 0.72	82.58 $\pm$ 0.53	82.36 $\pm$ 0.50	82.71 $\pm$ 0.50	82.44 $\pm$ 0.48	82.86 $\pm$ 0.55	82.65 $\pm$ 0.50
0.5	80.06 $\pm$ 0.74	80.05 $\pm$ 0.71	80.88 $\pm$ 0.72	80.59 $\pm$ 0.83	81.44 $\pm$ 0.64	81.26 $\pm$ 0.63	81.92 $\pm$ 0.22	81.63 $\pm$ 0.21	81.83 $\pm$ 0.32	81.59 $\pm$ 0.41
0.6	79.01 $\pm$ 0.61	78.86 $\pm$ 0.53	79.75 $\pm$ 0.60	79.49 $\pm$ 0.56	79.92 $\pm$ 0.79	79.86 $\pm$ 0.68	80.28 $\pm$ 0.19	80.07 $\pm$ 0.21	80.46 $\pm$ 0.28	80.16 $\pm$ 0.18
0.7	78.44 $\pm$ 0.31	78.16 $\pm$ 0.35	78.64 $\pm$ 0.75	78.46 $\pm$ 0.64	78.55 $\pm$ 1.16	78.45 $\pm$ 1.01	79.05 $\pm$ 0.23	78.71 $\pm$ 0.23	79.31 $\pm$ 0.35	78.95 $\pm$ 0.24

Table 13. Performance of MMGCN on IEMOCAP under different IMR settings when integrated with two variants of BALM.

IMR Settings	IEMOCAP				CMU-MOSEI			
	+BALM-D		+BALM-S		+BALM-D		+BALM-S	
	Acc	w-F1	Acc	w-F1	Acc	w-F1	Acc	w-F1
(0.3, 0.5, 0.7)	64.51	64.02	62.29	62.47	80.79	80.69	81.04	80.39
(0.3, 0.7, 0.5)	61.49	60.80	59.15	59.51	78.01	77.82	78.32	77.77
(0.5, 0.3, 0.7)	63.83	63.50	65.13	65.18	84.04	83.76	84.07	83.86
(0.5, 0.7, 0.3)	60.63	60.53	60.87	60.90	77.99	77.66	79.25	78.94
(0.7, 0.3, 0.5)	64.76	64.65	64.26	64.49	84.56	84.31	84.31	84.22
(0.7, 0.5, 0.3)	60.57	60.60	60.44	60.63	82.55	82.43	81.65	81.53

Table 14. Performance of BALM-M variant on IEMOCAP under different IMR settings.

MR Setting	GCNet <sub>+BALM-M</sub>		MMGCN <sub>+BALM-M</sub>		MMDFN <sub>+BALM-M</sub>	
	Acc	w-F1	Acc	w-F1	Acc	w-F1
(0.3, 0.5, 0.7)	59.46 $\downarrow$ 1.85	59.93	65.50 $\uparrow$ 1.11	65.26	69.01 $\uparrow$ 1.67	68.79
(0.3, 0.7, 0.5)	58.23 $\uparrow$ 0.87	58.47	60.57 $\uparrow$ 0.50	60.69	64.08 $\uparrow$ 0.68	63.54
(0.5, 0.3, 0.7)	61.43 $\uparrow$ 0.12	61.57	65.13 $\downarrow$ 0.24	65.19	69.32 $\uparrow$ 0.56	69.06
(0.5, 0.7, 0.3)	56.87 $\downarrow$ 0.77	57.12	60.63 $\downarrow$ 1.66	60.68	64.39 $\uparrow$ 0.37	64.10
(0.7, 0.3, 0.5)	58.16 $\downarrow$ 1.17	58.31	63.89 $\downarrow$ 1.11	63.90	68.45 $\uparrow$ 1.23	68.29
(0.7, 0.5, 0.3)	54.71 $\downarrow$ 5.55	54.97	61.18 $\downarrow$ 0.56	61.25	65.13 $\downarrow$ 1.37	64.70

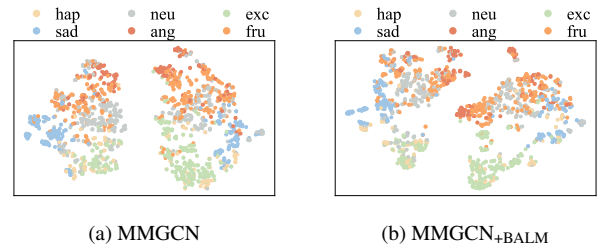
## F.7. Shared- and Imbalanced Missing Rates Relation

Given a dataset of  $N$  samples with  $M$  modalities, and the binary observation indicator  $e_i^m$  of modality  $m$  for sample  $i$  with  $e_i^m = 0$  denotes missing. Following [7, 19], the shared

$$r_{\text{shared}} = \frac{\sum_{m=1}^M \sum_{i=1}^N (1 - e_i^m)}{MN}, \quad (37)$$

Table 15. Performance of BALM-M variant on CMU-MOSEI under different IMR settings.

MR Setting	GCNet <sub>+BALM-M</sub>		MMGCN <sub>+BALM-M</sub>		MMDFN <sub>+BALM-M</sub>	
	Acc	w-F1	Acc	w-F1	Acc	w-F1
(0.3, 0.5, 0.7)	81.70 $\uparrow$ 0.16	81.44	81.29 $\downarrow$ 0.74	80.69	81.40 $\downarrow$ 0.66	80.96
(0.3, 0.7, 0.5)	78.59 $\uparrow$ 0.08	78.10	78.40 $\downarrow$ 0.33	78.10	77.44 $\downarrow$ 1.37	77.34
(0.5, 0.3, 0.7)	82.83 $\downarrow$ 0.44	82.66	82.97 $\uparrow$ 1.57	82.97	83.65 $\downarrow$ 0.69	83.55
(0.5, 0.7, 0.3)	77.55 $\downarrow$ 1.95	77.54	77.96 $\downarrow$ 1.87	78.00	78.70 $\downarrow$ 0.66	78.50
(0.7, 0.3, 0.5)	82.97 $\downarrow$ 0.66	82.96	84.26 $\downarrow$ 0.58	84.07	84.48 $\downarrow$ 0.30	84.36
(0.7, 0.5, 0.3)	81.15 $\downarrow$ 0.94	81.11	82.72 $\uparrow$ 0.22	82.29	82.31 $\downarrow$ 0.22	82.16

Figure 10. The multimodal fusion (i.e.,  $h$  in Eq. 12) corresponding to the inputs from Fig. 8, colored by ground truth.

missing rate is defined as:

while the modality-specific missing rate under IMR is given by:

$$r_m = \frac{\sum_{i=1}^N (1 - e_i^m)}{N}. \quad (38)$$

Thus, we can assume the IMR settings equivalent to a given SMR are those that satisfy

$$\sum_{m=1}^M r_m = Mr_{\text{shared}}. \quad (39)$$

Accordingly, in Fig. 2 of the main paper, we compare the performance of models addressing missing modalities under  $SMR = 0.5$  with IMR configurations satisfying  $r_A + r_L + r_V = 1.5$ . The detailed results are provided in Table 1 for the sampled IMR settings and in Table 11 for  $SMR = 0.5$ . These experiments show that a shared missing rate alone cannot fully capture a model’s behavior, particularly under highly imbalanced missing-rate conditions, underscoring the necessity of investigating IMR scenarios.

### F.8. Modality Discrepancies

In this section, we provide extended visual comparisons of modality discrepancies for MMGCN vs. MMGCN+BALM and MMDFN vs. MMDFN+BALM on IEMOCAP under different IMR configurations (from Fig. 11 to Fig. 22).

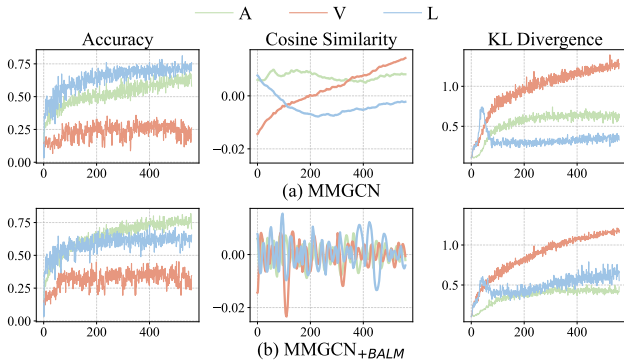


Figure 11.  $(r_A, r_L, r_V) = (0.3, 0.5, 0.7)$

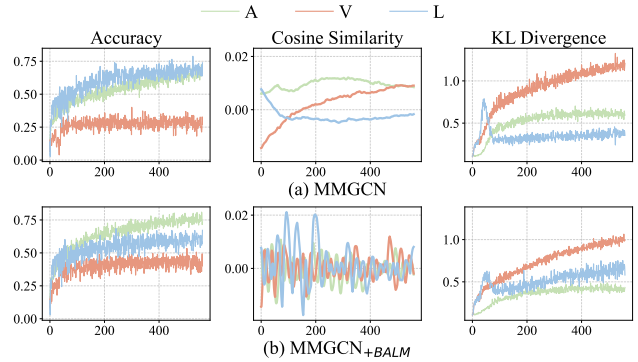


Figure 12.  $(r_A, r_L, r_V) = (0.3, 0.7, 0.5)$

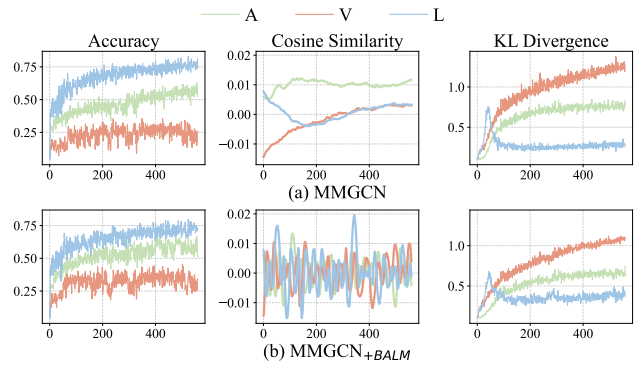


Figure 13.  $(r_A, r_L, r_V) = (0.5, 0.3, 0.7)$

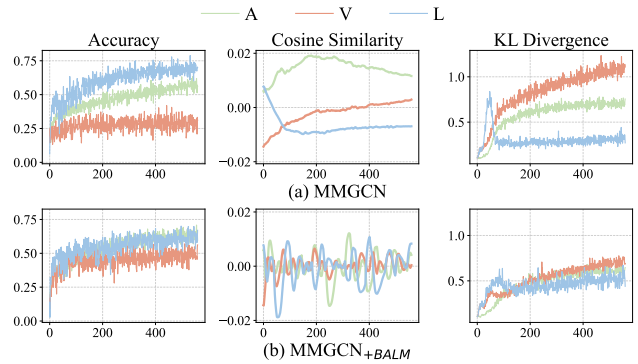


Figure 14.  $(r_A, r_L, r_V) = (0.5, 0.7, 0.3)$

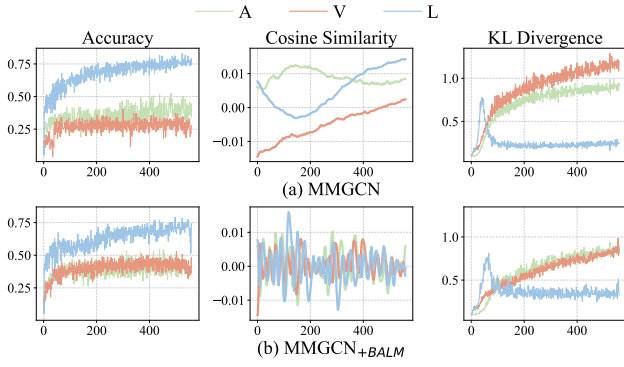


Figure 15.  $(r_A, r_L, r_V) = (0.7, 0.3, 0.5)$

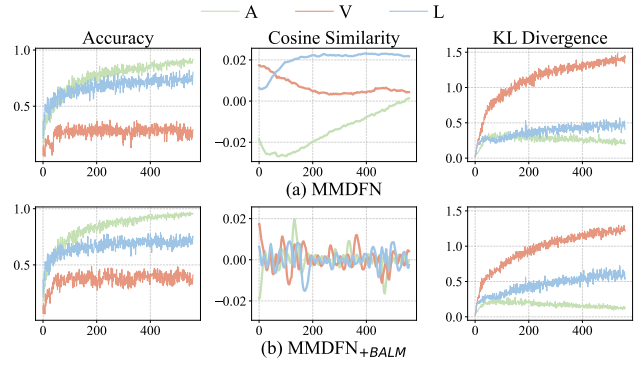


Figure 18.  $(r_A, r_L, r_V) = (0.3, 0.7, 0.5)$

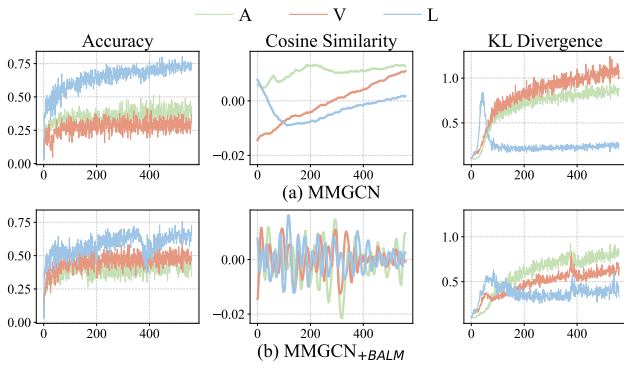


Figure 16.  $(r_A, r_L, r_V) = (0.7, 0.5, 0.3)$

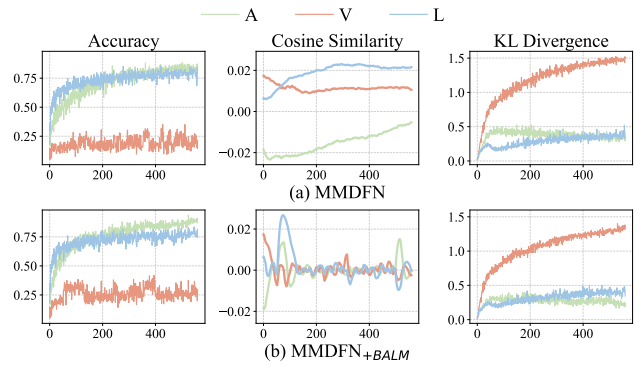


Figure 19.  $(r_A, r_L, r_V) = (0.5, 0.3, 0.7)$

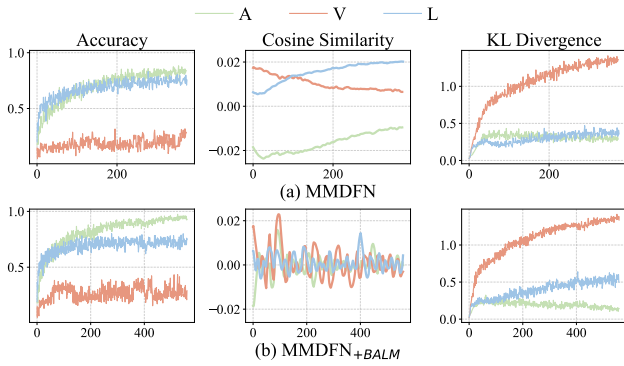


Figure 17.  $(r_A, r_L, r_V) = (0.3, 0.5, 0.7)$

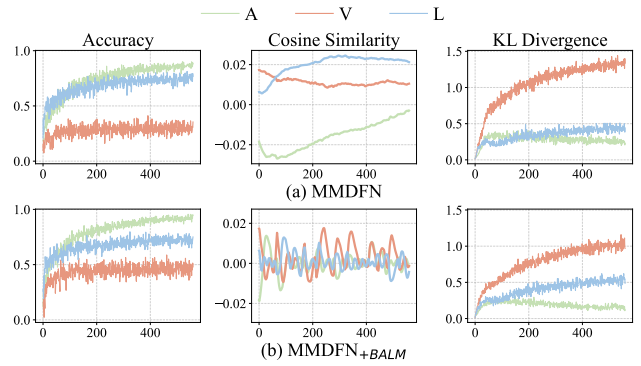


Figure 20.  $(r_A, r_L, r_V) = (0.5, 0.7, 0.3)$

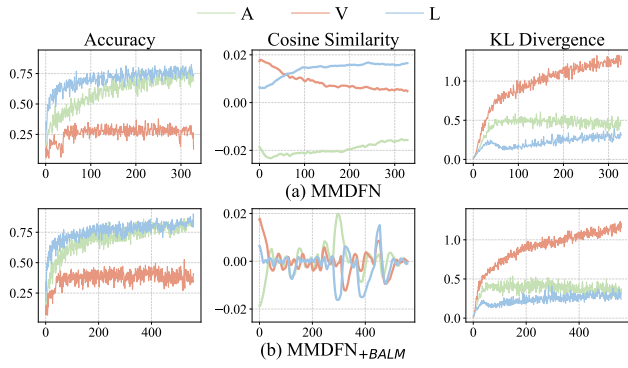


Figure 21.  $(r_A, r_L, r_V) = (0.7, 0.3, 0.5)$

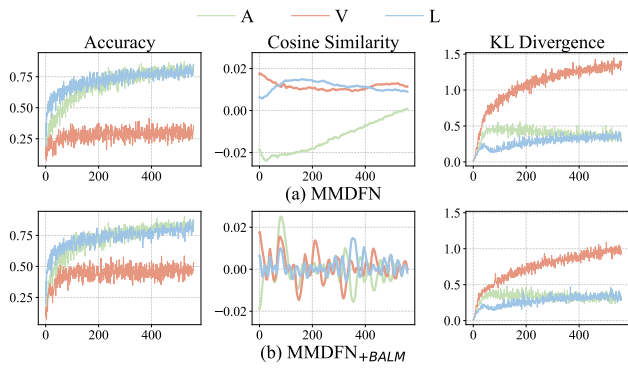


Figure 22.  $(r_A, r_L, r_V) = (0.7, 0.5, 0.3)$